Chemical Geology 401 (2015) 28–42

Contents lists available at ScienceDirect

Chemical Geology

journal homepage: www.elsevier.com/locate/chemgeo

Integrated O–Sr–Nd isotope constraints on the evolution of four important Fe–Ti oxide ore-bearing mafic–ultramafic intrusions in the Emeishan large igneous province, SW China

Song-Yue Yu [a], Xie-Yan Song [a,*], Edward M. Ripley [b], Chusi Li [b], Lie-Meng Chen [a], Yu-Wei She [a], Yan Luan [a]

[a] State Key Laboratory of Ore Deposit Geochemistry, Institute of Geochemistry, Chinese Academy of Sciences, 46th Guanshui Road, Guiyang 550002, PR China
[b] Department of Geological Sciences, Indiana University, 1001 East Tenth Street, Bloomington, IN 47405, USA

ARTICLE INFO

Article history:
Received 2 September 2014
Received in revised form 3 February 2015
Accepted 18 February 2015
Available online 26 February 2015

Editor: Catherine Chauvel

Keywords:
O–Sr–Nd isotopes
Crustal contamination
Fe–Ti oxide
Emeishan large igneous province
Layered intrusions

ABSTRACT

In the Emeishan large igneous province, SW China, there are many layered mafic–ultramafic intrusions such as the Baima, Hongge, Panzhihua and Taihe intrusions that host world-class Fe–Ti oxide ore deposits. Despite numerous studies, the origin of these deposits still remains elusive. This includes the role of crustal contamination, especially addition of external CO_2 from carbonate country rocks during contact metamorphism, in triggering Fe–Ti oxide crystallization from high-Mg basaltic magma. To address this important issue, we have carried out an integrated O–Sr–Nd isotope study of these ore-bearing intrusions and the country rocks. Our results show that in these intrusions clinopyroxene is much less susceptible to fluid–mineral oxygen isotope exchange than coexisting plagioclase and Fe–Ti oxides, which is similar to other intrusions worldwide (e.g., Taylor, 1967; Gregory and Taylor, 1981). Our calculations based on the least exchanged clinopyroxene oxygen isotope data show that the mean $\delta^{18}O$ values for the parental magmas of these intrusions are Baima = 5.7‰, Panzhihua = 6.1‰, Taihe = 5.9‰. The estimated mean $\delta^{18}O$ value for the parental magma of the Upper and Middle Zones of the Hongge intrusion is 6.2‰, which is similar to those for the parental magmas of the other intrusions (Baima, Panzhihua and Taihe). By contrast, the estimated mean $\delta^{18}O$ value for the parental magma of the Lower Zone of the Hongge intrusion is higher (6.9‰). This difference, together with higher initial $^{87}Sr/^{86}Sr$ ratios (0.7057 to 0.7076) and lower εNd_t values (−2.82 to −0.07) for this zone, can be attributed to higher degrees of contamination with siliceous crustal materials in this zone than elsewhere in this intrusion. Comparison of O–Sr–Nd isotope compositions between the intrusions and country rocks reveals that bulk assimilation of carbonate country rocks is negligible in all of these intrusions. Mixing calculations using the O–Sr–Nd isotope data are consistent with variable degrees of contamination with siliceous crustal materials in the intrusions: Panzhihua, <5%, Baima and Taihe, <10%, the Middle and Upper Zone of the Hongge intrusion, <10%, the Lower Zone of the Hongge intrusion, <15%. These percentages are maximum values and may be reduced if contamination was selective in nature, involving Sr- and Nd-bearing fluids or partial melts. Based on the oxygen isotope results, an iterative calculation with a CO_2/magma mass ratio = 1/1000 for each increment reveals that the Panzhihua magma reacted with <1 wt.% of CO_2 released from the footwall during contact metamorphism. This amount is not sufficient to increase the oxidation state of the magma to the level that Fe–Ti oxides would crystallize alone from the magma. Therefore, we conclude that external CO_2 did not play a major role in the formation of the Fe–Ti oxide ores in the Panzhihua intrusion.

1. Introduction

Fe–Ti oxides commonly crystallize at the late stages of magma differentiation in tholeiitic systems. This is evident from the occurrence of cumulus Fe–Ti oxide layers in the Upper Zone of the Bushveld Complex and the Middle Zone of the Skaergaard layered intrusion where olivine is absent or Fe-rich (Fo < 48 mol%) (e.g., Reynolds, 1985; McBirney, 1989). However, this is not the case for the Permian mafic–ultramafic layered intrusions in the Emeishan Large Igneous Province (ELIP), SW China. Concordant, thick massive Fe–Ti oxide layers and magnetite-rich gabbroic layers containing clinopyroxene with $Mg^{\#}$ from 75 to 85 and olivine with Fo values of 65–81 mol% in some places occur in the lower parts of these layered intrusions (Figs. 1, 2) (Pang et., 2009; Zhang et al., 2012; Song et al., 2013; Luan et al., 2014; She et al., 2014). This indicates relatively early Fe–Ti oxide saturation in these magmatic systems as compared to other large layered intrusions in the world. The reason for the early Fe–Ti oxide saturation in the ELIP

* Corresponding author at: Institute of Geochemistry, Chinese Academy of Sciences, 46th Guanshui Road, Guiyang, 550002, PR China. Tel.: +86 0851 5895538; fax: +86 0851 5891664.
E-mail address: songxieyan@vip.gyig.ac.cn (X.-Y. Song).

http://dx.doi.org/10.1016/j.chemgeo.2015.02.020
0009-2541/

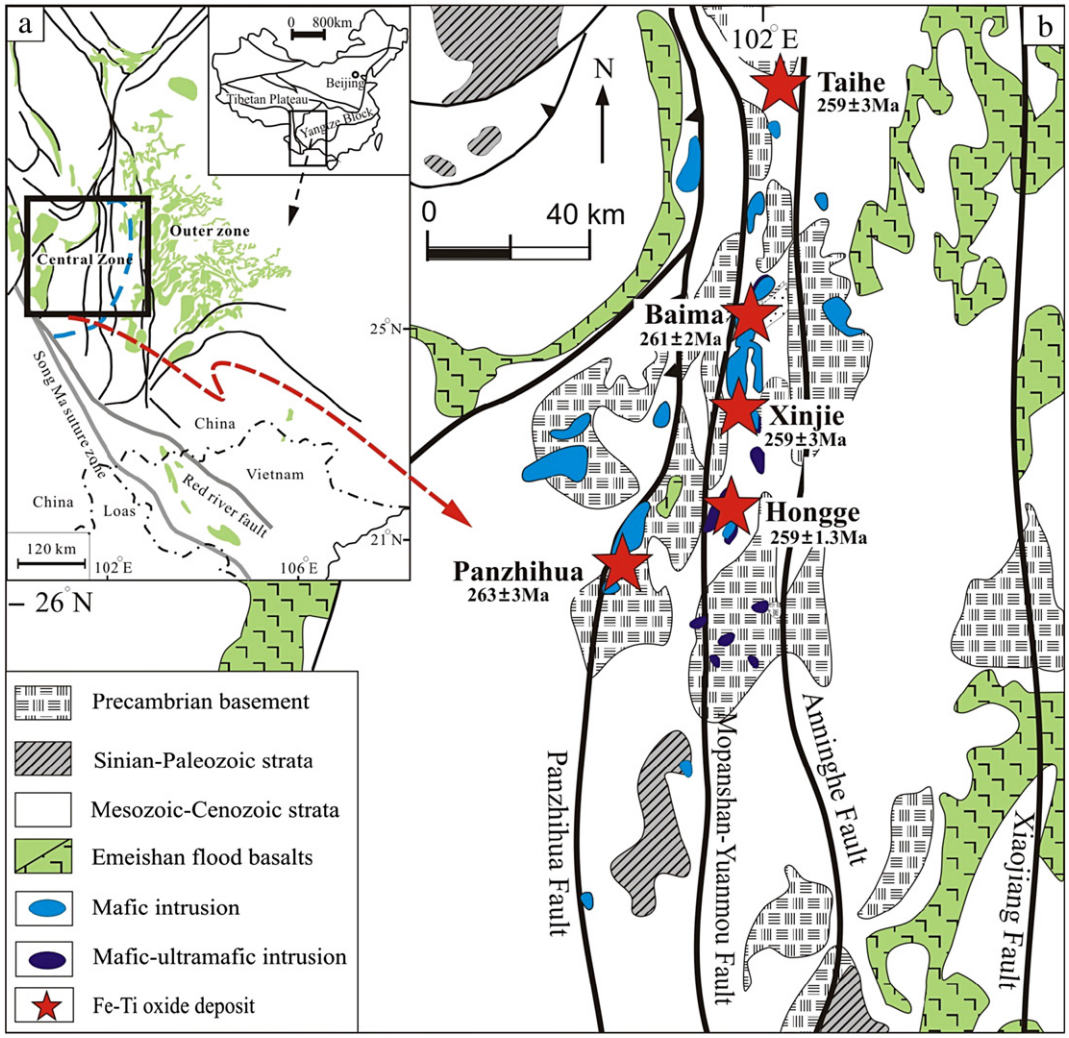

Fig. 1. (a) Distribution of Emeishan flood basalts. (b) Simplified geological map of the central part of the Emeishan large igneous province, with locations of Fe–Ti oxide ore-bearing mafic–ultramafic intrusions (modified after Song et al., 2009). The ages of the mafic–ultramafic intrusions are from Zhou et al. (2005, 2008) and Zhong et al. (2011).

mafic–ultramafic intrusions is not clear. Many researchers suggested that it is due to unusually high concentrations of Fe–Ti in the parental magmas that can be traced back to mantle-derived picritic magma by olivine fractional crystallization (Pang et al., 2008; Bai et al., 2012; Zhang et al., 2012; Song et al., 2013; Luan et al., 2014; She et al., 2014). Ganino et al. (2008) proposed that in the case of the Panzhihua intrusion, Fe–Ti oxide crystallization immediately after emplacement was due to oxidation of basaltic magma by CO_2-rich fluids released from dolomite country rocks during contact metamorphism (Fig. 2). It is clear that such an in-situ mass transfer model is not applicable to the Hongge deposit because the massive Fe–Ti oxide ore zones in this intrusion are not in direct contact with dolomites (Fig. 2). However, previous contamination with dolomite country rocks during magma ascent or ponding at depth is still a possibility. At Hongge, hydration of magma by external H_2O released from footwall meta-sandstones during contact metamorphism is another possibility for the concurrent crystallization of Fe-Ti oxides from the contaminated magma; the thick oxide layers in the Hongge intrusion may have formed by this process coupled by multiple magma replenishment and crystal sorting in a magma flow-through system (Luan et al., 2014). In addition, some researchers believed that the Fe–Ti oxide orebodies in the ELIP layered intrusions formed by liquid immiscibility (Wang and Zhou, 2013; Zhou et al., 2013; Liu et al., 2014). To evaluate these competing models, we have carried out an integrated O–Sr–Nd isotope study of four representative Fe–Ti oxide ore-bearing mafic–ultramafic intrusions (Baima, Hongge, Panzhihua and Taihe) in the ELIP.

2. Geological background

Southwestern China comprises the Yangtze Block in the east and the Tibetan Plateau in the west (Fig. 1). The basement of the Yangtze block consists of Paleo-Mesoproterozoic low to medium grade meta-sedimentary and meta-volcanic rocks, which are overlain by sedimentary strata of Neoproterozoic to early-Permian ages. The Neoproterozoic strata are predominantly composed of dolomites and sandstones (Liu, 1991). Neoproterozoic granites and high-grade metamorphic complexes are present in places in the western and northern margins of the Yangtze block (Zhou et al., 2002a).

The Emeishan large igneous province (ELIP), which is composed of voluminous flood basalts and numerous small mafic–ultramafic intrusions, occurs in SW China and northern Vietnam (Fig. 1, Chung and Jahn, 1995; Xu et al., 2001; Song et al., 2001, 2004; Zhou et al., 2002b). The flood basalts in the ELIP cover an area > 5×10^5 km^2. The total thicknesses of the volcanic sequence are up to ~2000 m (Xu et al., 2004; Song et al., 2008a). The ELIP is further divided into the central and outer zone. Both low-Ti and high-Ti basalts are present in the central zone. In contrast, the volcanic rocks in the outer zone are dominated by high-Ti basalts (Xu et al., 2001; Xiao et al., 2004). Radiometric dating of the associated mafic–ultramafic intrusions gives an age of magmatism at ~260 Ma for the ELIP, which is roughly contemporaneous with the global end-Guadalupian mass extinction (Ali et al., 2002; Zhou et al., 2002b).

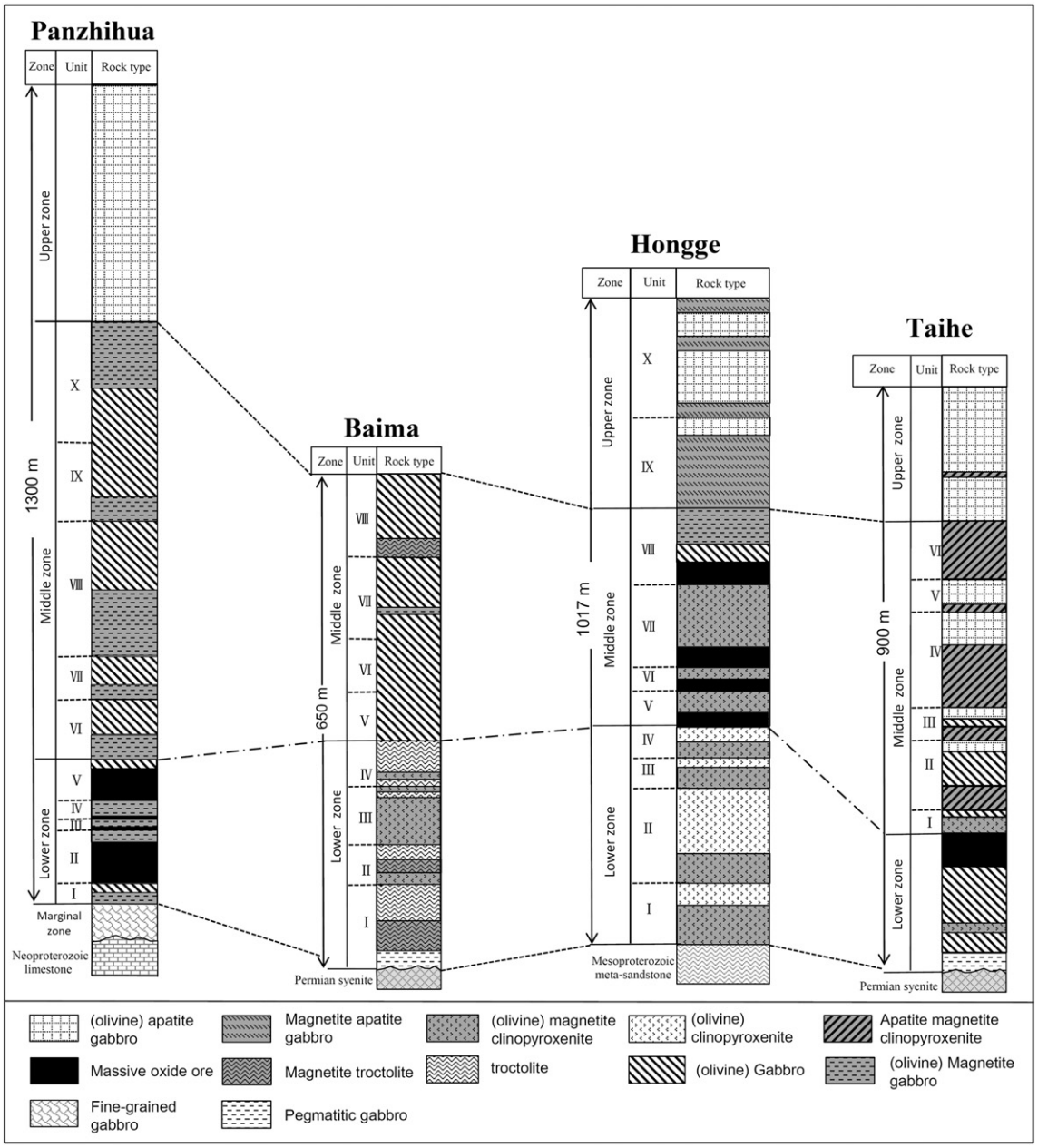

Fig. 2. Lithological comparison of several important Fe–Ti oxide ore-bearing mafic–ultramafic intrusions in the Emeishan large igneous province (modified from Song et al., 2013; Luan et al., 2014; She et al., 2014).

Many mafic–ultramafic intrusions are exposed in the central zone of the ELIP due to severe uplifting and erosion. Their distribution is controlled by the N–S trending regional faults (Fig. 1). Some of these intrusions, such as Baima, Hongge, Panzhihua and Taihe host important Fe–Ti–V oxide ore deposits. The total reserve of these four deposits together exceeds 10 billion tons of ores with 25–35 wt.% Fe, 4–13 wt.% Ti and 0.1–0.45 wt.% V (Panxi Geological Unit, 1984). One of the coeval mafic–ultramafic intrusions in the region, the Xinjie intrusion, also contains important Ni–Cu–PGE sulfide mineralization (Zhong et al., 2004; Wang et al., 2008). In addition, a few other coeval intrusions in the region, such as Baimazhai, Limahe and Jinbaoshan, host economically valuable Ni–Cu–PGE sulfide deposits (Tao et al., 2007, 2008; Song et al., 2008b).

3. Petrology of the four selected intrusions

The Panzhihua and Taihe intrusions are mafic layered intrusions, whereas the Baima and Hongge are mafic–ultramafic layered intrusions (Fig. 2). The petrological characteristics of these intrusions are described in detail by previous researchers (Zhong et al., 2002; Zhou et al., 2005; Pang et al., 2008; Zhang et al., 2012; Song et al., 2013; Luan et al., 2014; She et al., 2014). Here only brief summaries are given.

The Panzhihua intrusion is predominantly composed of gabbros (Fig. 2). The surface exposure of the Panzhihua intrusion is ~19 km in length. It dips northwest at angles ranging from 40° to 60°. It was emplaced into Neoproterozoic dolomitic limestones. Contact metamorphism produced up to 300 m-thick forsterite and diopside marbles in the lower contact (Fig. 3a). Elsewhere the intrusion is in faulted contact with late-Permian syenites and Triassic terrestrial clastic sedimentary rocks. The Panzhihua intrusion is further divided into the Marginal, Lower, Middle and Upper Zones. Most important Fe–Ti oxide layers occur in the Lower Zone.

The Baima intrusion is predominantly composed of gabbros and troctolites (Fig. 2). It is ~24 km in length and ~2 km in thickness. The intrusion dips at 50–70° to the west. It was emplaced into Neoproterozoic

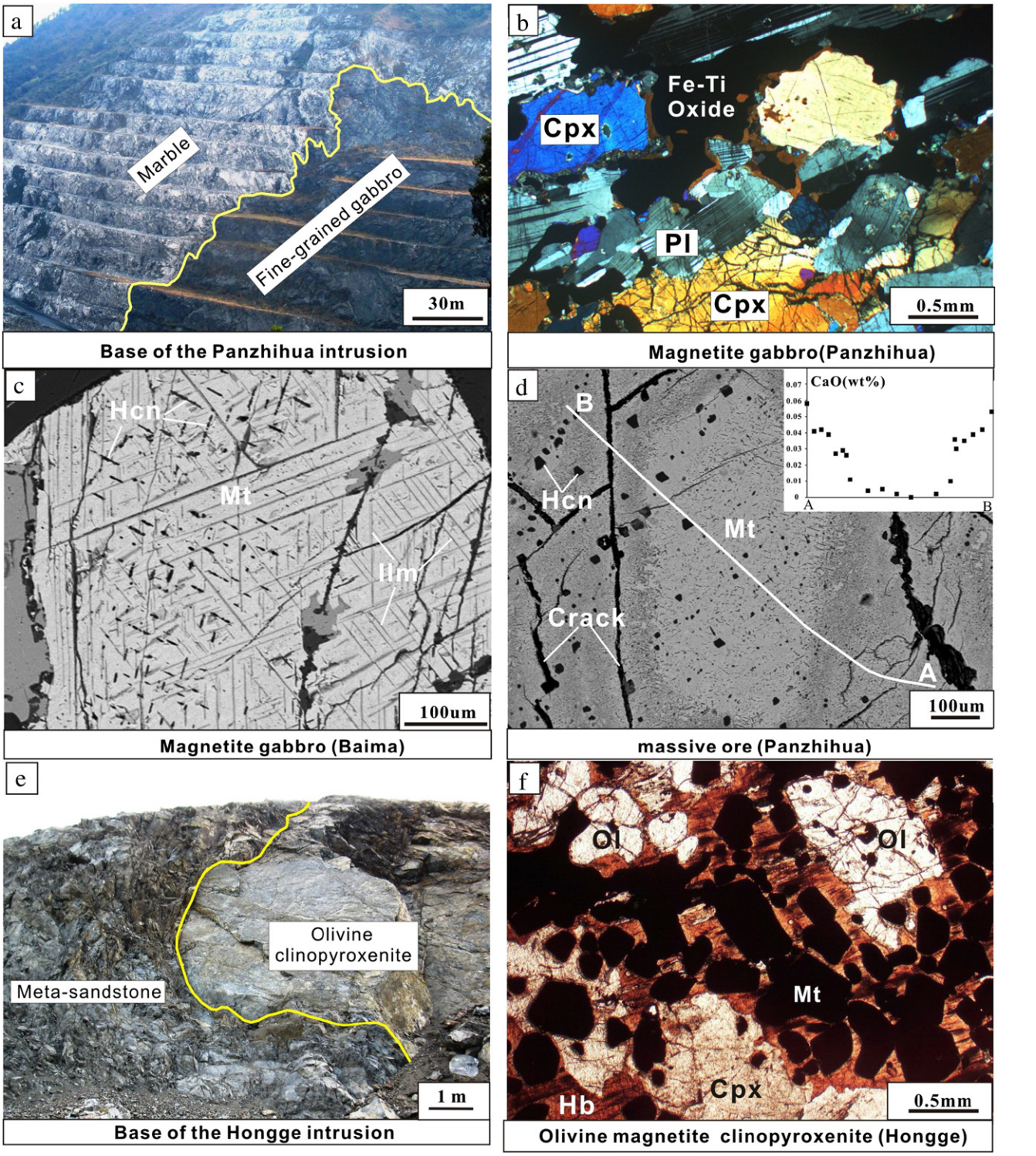

Fig. 3. (a) Field photo showing the irregular contact between fine-grained gabbro and Proterozoic marble footwall rocks, Panzhihua intrusion. (b) Microphotograph of Fe–Ti oxide-bearing gabbro in the Middle Zone of the Panzhihua intrusion. (c) Microphotograph showing typical exosolution texture of Fe–Ti spinel in the oxide-rich gabbro in the lower zone of the Baima intrusion. (d) Microphotograph showing a fractured and altered magnetite crystal from the lower zone of the Panzhihua intrusion. (e) Field photo of olivine clinopyroxenite in contact with the Proterozoic meta-sandstone footwall rocks of the Hongge intrusion. (f) Microphotograph showing abundant magnetite inclusions enclosed in clinopyroxene crystal and hornblende oikocrysts in the lower zone of the Hongge intrusion. Cpx: clinopyroxene, Hb: hornblende, Hcn: hercynite, Ilm: ilmenite, Mt: magnetite, Ol: olivine, Pl: plagioclase.

dolomitic limestones and Cambrian clastic sediments. Large marble and schist xenoliths are common in the intrusion. The intrusion was intruded by syenites and granites. The Baima intrusion is further divided into the Lower and Middle zones. Pegmatitic gabbros occur in places at the base of the intrusion (Fig. 2, Zhang et al., 2012). Unlike the Panzhihua intrusion, no massive Fe–Ti oxide layers are present in the Baima intrusion. Important Fe–Ti–V oxide mineralization occurs as magnetite-rich troctolite layers in the lower zone of the intrusion (Fig. 2).

The Taihe and Hongge mafic–ultramafic intrusions are similarly composed of clinopyroxenites and gabbros. The Hongge intrusion is

an elongated lopolith which is ~16 km in length and 3–6 km in width (Panxi Geological Unit, 1984). The country rocks of the intrusion are Mesoproterozoic schists and meta-sandstones in the north (Fig. 3e), Neoproterozoic dolomitic limestones in the south, and the Emeishan flood basalts in the northeast (Luan et al., 2014). In some places the intrusion is in contact with younger granite and syenite (255.2 ± 3.6 Ma, Xu et al., 2008). The Hongge intrusion is further divided into the Lower, Middle and Upper Zones (Fig. 2). The most important Fe–Ti oxide mineralization occurs as thick, massive layers in the Middle Zone.

The Taihe intrusion is ~3 km in length, ~2 km in width and ~1.2 km in thickness. It dips to the southeast with angles of 50–60°. Diopside–garnet marble xenoliths are common in the Taihe intrusion (Panxi Geological Unit, 1984). The immediate country rocks of the intrusion are contemporaneous syenites (261 ± 2 Ma, Xu et al., 2008). The Taihe intrusion is further divided into Lower, Middle and Upper Zones (Fig. 2). Important Fe–Ti oxide mineralization in the intrusion occurs as Fe–Ti oxide-rich layers throughout the intrusion as well as a thick massive oxide layer in the upper part of the Lower Zone. In the Panzhihua, Baima and Hongge intrusions abundant apatite occurs most commonly in their upper zones. In contrast, in the Taihe intrusion abundant apatite occurs in its middle zone as well as its upper zone (She et al., 2014).

All of these intrusions have been variably affected by postmagmatic hydrothermal alteration. The most extensive alteration occurs in the fractured zones. The representative textures of the least-altered rocks and oxide ores from these intrusions are given in Fig. 3b–c. The typical texture of a pristine gabbroic sample from the Panzhihua intrusion is shown in Fig. 3b. As shown by an oxide ore sample from the Baima intrusion, exsolution lamellae of ilmenite and hercynite in the magnetite crystal are common in the oxide layers in these intrusions (Fig. 3c). In the associated silicate rocks, clinopyroxene crystals commonly contain small magnetite exsolution lamellae (Zhang et al., 2012; Song et al., 2013). Chemical compositions of magnetite from the massive ores of the Panzhihua and Taihe intrusions were partially changed due to infiltration of external fluid along the cracks (Fig. 3d). In the Lower Zone of the Hongge intrusion where abundant magmatic hornblende and biotite (5–15% together) are present, magnetite commonly occurs as euhedral crystals enclosed in clinopyroxene or hornblende oikocrysts (Fig. 3f).

4. Sampling and analytical procedures

A total of nearly 200 oxygen isotope measurements were made on whole rocks and mineral separates (clinopyroxene, plagioclase and Fe–Ti oxides) from the Panzhihua, Baima, Hongge and Taihe intrusions, and some footwall rocks. Magnetic separation was followed by hand-picking under a microscope. The mineral separates and whole-rock samples were crushed to 60–100 mesh powders. The powders were baked at 120 °C in vacuum for at least >24 h before oxygen extraction using a conventional BrF_5 extraction system. A powder sample of 5 to 8 mg was placed in a Ni-reaction vessel and heated overnight with BrF_5 at ~600 °C (Clayton and Mayeda, 1963). The released oxygen was converted to CO_2 by reaction with heated graphite disks wrapped with Pt–Rh wires. The CO_2 gas was analyzed on a Finnigan Delta-Plus stable isotope ratio mass spectrometer in the Stable Isotope Research Facility of Indiana University. The analytical precision of single $\delta^{18}O$ measurement is ±0.05‰ (2σ), with a sample reproducibility of ±0.2‰ (2σ). Results are reported in standard delta notation relative to VSMOW (Table 1). The NBS-28 quartz has a value of 9.6 ± 0.2‰ in the Indiana University laboratory.

The concentrations of major elements in the rock samples were determined using a PANalytical Axios X-ray fluorescence spectrometer (XRF) on fused glass beads at the ALS Chemex (Guangzhou) Co., Ltd. with an analytical uncertainty less than 5%. 0.7 g of powder from each sample was mixed completely with $Li_2B_4O_7$–$LiBO_2$ flux and then fused to a glass bead at 1050–1100 °C in an automatic melting instrument. Loss on ignition (LOI) was obtained from 1 g powdered sample that was heated up to 1100 °C for 1 h. Table A1 lists the results for Canadian reference material STSD-4 and South African reference material SARM-45 determined as unknowns. Our results are in good agreement with the compiled values of Govindaraju (1994). The abundances of trace elements in the rocks were determined using a Perkin-Elmer Sciex ELAN 6000 ICP-MS at the Institute of Geochemistry, Chinese Academy of Sciences (IGCAS). The powdered samples (50 mg) were dissolved in Hf + HNO_3 solution in high-pressure Teflon bombs that were heated at ~190 °C for 12 h (Qi et al., 2000). Rh was used as an internal standard to monitor signal drift during analysis. The USGS standard AGV-2 was determined as an unknown. This standard was run with every batch of samples. Replicate analysis of AGV-2 typically gave an overall analytical precision of better than 5% relative to the recommended values (Wilson, 1998).

For Sr–Nd isotopic analyses, powders of selected, relatively fresh whole-rock samples from the Baima intrusion and important footwall rocks of the four selected mafic–ultramafic intrusions in the ELIP were dissolved in the HF–HNO_3 solution in Savillex screwtop Teflon beakers at 150 °C for 10 days. Sr and REE were separated in columns made of Sr and REE resins from the Eichrom Company using 0.1% HNO_3 as an elutant. Separation of Nd from the REE fractions was carried out in the HDEHP columns using 0.18 N HCl as an elutant. The Sr–Nd isotopic compositions of the samples were determined using a Micromass Isoprobe Multi-Collector ICPMS at Guangzhou Institute of Geochemistry, Chinese Academy of Sciences. The results are shown in Table A2. The results of the standards analyzed together with the samples are: the NBS987 international standard, $^{87}Sr/^{86}Sr = 0.710262 \pm 17$ (recommended value, 0.710250 ± 10, McArthor, 1994); the Sr-GIG internal standard, $^{87}Sr/^{86}Sr = 0.708844 \pm 23$; the JNdi-1 international standard, $^{143}Nd/^{144}Nd = 0.512123 \pm 10$ (recommended value, $^{143}Nd/^{144}Nd = 0.512115 \pm 7$, Tanaka et al., 2000); the Nd-GIG internal standard, $^{143}Nd/^{144}Nd = 0.511525 \pm 10$. εNd values were calculated based on an age of 260 Ma, decay constants of 6.54×10^{-12} ($year^{-1}$) for ^{147}Sm, and present day chondritic values of $^{143}Nd/^{144}Nd = 0.512630$, $^{147}Sm/^{144}Nd = 0.1960$ (Bouvier et al., 2008).

5. Results

5.1. Oxygen isotope compositions of mineral separates

The oxygen isotope compositions of plagioclase, clinopyroxene and Fe–Ti oxide separated from the Baima, Hongge, Panzhihua and Taihe Fe–Ti oxide ore-bearing layered mafic–ultramafic intrusions are listed in Table 1. The differences of replicated analyses for clinopyroxene and Fe–Ti oxide separates from twelve samples are less than 0.3‰, which is within the range of typical analytical deviation. The stratigraphic variations of $\delta^{18}O$ values for the mineral separates are shown in Fig. 4. For comparison, calculated $\delta^{18}O$ values for hypothetical minerals which crystallize from an uncontaminated mantle-derived magma with oxygen isotopic composition assumed to be the same as that of the average oceanic island basalt (OIB, 6.0 ± 0.7‰ given by Eiler et al., 1997) are shown as gray, brown and yellow bands, respectively. As shown in Fig. 4, no systematic variations of mineral oxygen isotope compositions with depths are present in the Baima, Panzhihua and Taihe intrusions. In the Hongge intrusion, the $\delta^{18}O$ values of clinopyroxene tend to be lower in the Middle and Upper Zones than in the Lower Zone, which generally coincides with significant changes in the abundances of Fe–Ti oxides (indicated by whole-rock $Fe_2O_3^T$) and apatite (indicated by whole-rock P_2O_5).

Except four samples which have anomalously high $\delta^{18}O$ values from 6.9 to 8.8‰, the other 43 samples of clinopyroxene separates from the Baima, Panzhihua and Taihe intrusions have $\delta^{18}O$ values ranging from 4.8 to 6.6‰, with an average of 5.5‰ (n = 43). The average value is similar to the estimated value for the hypothetical clinopyroxene that may crystallize from the uncontaminated mantle-derived magma with oxygen isotopic composition the same as that of OIB. The $\delta^{18}O$ values

Table 1
Oxygen isotope data for important Fe–Ti oxide ore-bearing mafic–ultramafic intrusions in the ELIP and their footwall rocks.

Sample no.	Rock type[a]	Locality	Unit	Hight from the base (m)	$\delta^{18}O_{cpx}$[b]		$\delta^{18}O_{pl}$[b]	$\delta^{18}O_{oxd}$[b]		$\delta^{18}O_{(whole\ rock)}$	$\delta^{18}O_{magma}$[c]	Δ_{pl-Cpx}[b]	$\Delta_{Cpx-oxd}$[b]
Panzhihua intrusion													
Zhujiabaobao segment													
SP05-1	OXG	Lower zone	I	5	5.7		7.9	2.2			6.2	2.2	3.5
SP05-3	Gabbro		I	11	5.7		8.6	1.2			6.2	3.0	4.5
SP05-4	MOO		II	31				2.6					
SP05-5	MOO		II	40				1.8					
SP05-7	MOO		II	85				1.9					
SP05-8	OXG		II	95	5.4			1.3			5.9		4.1
SP05-10	Gabbro		II	114	5.3		5.1	3.9			5.8	−0.3	1.4
SP05-15	Gabbro		IV	138	6.0		4.7	2.6			6.5	−1.3	3.4
SP05-17	OXG		IV	155	5.5[f]	5.5[f]	7.7	2.5			6.0	2.3	3.0
SP05-20	MOO		V	190				1.2					
SP05-21	MOO		V	215				1.2					
SP05-23	Gabbro	Middle zone	VI	285	8.0[f]	7.9[f]	9.4	2.5[f]	2.4[f]		8.5	1.5	5.4
SP05-26	OXG		VII	335	5.4		9.4	2.5			5.9	4.0	2.9
SP05-27	Gabbro		VII	355	5.1		9.7	2.1			5.6	4.7	3.0
SP05-28	OXG		VII	400	6.3		1.8	2.2			6.8	−4.6	4.1
SP05-35	OXG		IX	615	5.8		4.8	3.0			6.3	−1.0	2.8
SP05-39	Gabbro		IX	705	5.5		6.1	1.4			6.0	1.0	3.7
SP05-41	Gabbro		X	765	5.1		5.6	1.3			5.6	0.5	3.8
SP05-42	Gabbro		X	805	6.4		8.3	1.4			6.9	1.8	5.0
SP11-504	APG	Upper zone		1060	5.2[f]	5.2[f]	6.0	4.0			5.7	0.8	1.3
SP11-506	APG			1200	5.6		6.7	4.2[f]	4.2[f]		6.1	1.2	1.4
Daomakan segment													
SP10-55	SMOO	Lower zone	II	2.2			7.1	4.9					
SP10-57	MOO		II	3			5.7	3.6					
SP10-59	MOO		II	3.5			3.6	1.2					
SP10-70	SMOO		III	18				4.1					
SP10-71	MOO		III	20				5.0					
Nalajing segment													
PN11-65-1	MOO	Lower zone	I	0				2.8					
PN11-65	MOO		I	11				2.6					
PN11-64	MOO		I	24				2.8					
PN11-63	MOO		I	35				2.0					
Baima intrusion													
SB11-33	OXTR	Lower zone	I	22	5.5		6.3	2.5			5.7	0.8	3.0
SB11-21	OXTR		I	36	5.3[f]	5.2[f]	3.7	0.7			5.5	−1.6	4.7
SB11-15	TROC		I	54	5.9			0.8			6.1		
SB11-13	OXCP		II	100	5.5[f]	5.7[f]		2.2			5.7		
SB11-16	OXCP		III	192	5.2[f]	5.2[f]	6.2	1.4			5.4	1.0	3.8
SB11-24	TROC		IV	268	5.0		3.4	1.8			5.2	−1.6	3.2
SB11-27	OXCP		IV	283	5.4		6.0	1.7			5.6	0.6	3.7
SB11-30	OXG	Middle zone	V	345	5.3		7.1	1.6			5.8	1.8	3.7
SB11-45	OXG		VI	405	5.4		7.8	3.7			5.9	2.4	1.7
SB11-09	Gabbro		VI	421	5.7		6.6	−0.5			6.2	0.9	6.2
SB11-25	OLG		VII	450	5.5		7.9	3.8			6.0	2.4	1.7
SB11-28	OLG		VII	467	8.8		6.5	1.9			9.3	−2.3	6.9
SB11-42	OXG		VII	483	8.3[f]	8.2[f]	6.4	1.9			8.8	−1.9	6.4
SB11-08	Gabbro		VII	526	5.3		5.3	3.2[f]	3.2[f]		5.8	0.0	2.0
SB11-07	OLG		VII	544	4.8			3.2			5.3		
SB11-35	Gabbro		VII	587	5.0		5.6	2.0			5.5	0.6	3.0
Taihe intrusion													
ST11-46	OLG	Lower zone		0	5.2			2.7			5.7		2.5
ST11-44	Gabbro			32	5.5			2.6			6.0		2.9
ST11-42	OLG			67	5.4			1.4			5.9		4.0
ST11-34	MOO			143				0.7[f]	0.8[f]				
ST11-30	Gabbro	Middle zone	I	183	5.5			2.6			6.0		2.9
ST11-29	OXCP		II	194	5.5			1.9			5.7		3.6
ST11-27	OXCP		II	218	6.9			0.8			7.0		6.1
ST11-25	Gabbro		II	242	5.4			2.4			5.9		3.0
ST11-21	OXCP		III	296	5.1			1.9			5.3		
ST11-17	OXCP		IV	365	5.6			2.8			5.8		2.8
ST11-16	OXCP		IV	381	5.5			3.3			5.7		2.2
ST11-13	OXCP		IV	428	6.6			1.8			6.8		4.8
ST11-09	OXCP		V	490	5.7			2.2			5.9		3.6
ST11-06	OXCP		VI	548	5.7			4.2			5.9		1.4
ST11-48	Gabbro	Upper zone		655	5.7						6.2		
ST11-51	OXCP			698	6.0[f]	6.3[f]		3.2			6.2		2.8
Hongge intrusion													
SH10-77	OLCP	Lower zone	I	29	6.4			3.3			6.6		3.1

(continued on next page)

Table 1 (*continued*)

Sample no.	Rock type[a]	Locality	Unit	Hight from the base (m)	$\delta^{18}O_{cpx}$[b]	$\delta^{18}O_{pl}$[b]	$\delta^{18}O_{oxd}$[b]	$\delta^{18}O_{(whole\ rock)}$	$\delta^{18}O_{magma}$[c]	Δ_{pl-Cpx}[b]	$\Delta_{Cpx-oxd}$[b]
SH10-94	OLCP		III	257	6.8		3.4		7.0		3.4
SH10-96	OLCP		III	282	6.9		3.7		7.1		3.2
SH10-100	OXCP		IV	325	6.6		4.2		6.8		2.4
SH10-72	OXCP	Middle zone	VI	421	5.9[f] 5.8[f]		2.3		6.1		3.6
SH10-22	OXCP		VII	474	5.6		2.6		5.8		3.1
SH10-26	OXCP		VII	555	5.8		1.2		6.0		4.6
SH10-204	OXG		VII	604			3.2				
SH10-32	OXG		VII	618	5.7		4.3		6.2		1.4
SH10-69	OXG	Upper zone	IX	694			4.4				
SH10-68	OXG		IX	720	5.8		0.3		6.3		5.4
SH10-65	OXG		IX	778			2.6				
SH10-64	OXG		IX	796	6.0		3.1		6.5		2.8
SH10-54	Gabbro		X	947			2.8				
Footwall rocks[g]											
SP10-1	Schist	Panzhihua						11.3			
PN11-116	Schist							7.9			
PN11-113	MESD							11.7			
PN11-114	MESD							14.3			
SP10-27[d]	Marble							10.5			
SP10-28[d]	Marble							10.4[f] 8.3[f]			
SP10-29[d]	Marble							13.2			
PN11-115[e]	Marble							7.4			
SH10-40	MESD	Hongge						17.0			
SH10-73	MESD							16.6[f] 15.0[f]			
SH10-74	MESD							15.2			
SB09-7	SIMAR	Baima						11.6			
SB11-213	SIMAR							9.0			
SB11-230	SIMAR							11.2			
SB11-231	SIMAR							12.6			

[a] OXG, magnetite gabbro; APG, apatite gabbro; OLG, olivine gabbro; OLOXG, olivine–magnetite gabbro; MOO, massive oxide ore, TROC, troctolite; OXTR, magnetite troctolite; SMOO, semi-massive oxide ore; OXCP, magnetite clinopyroxenite; OLCP, olivine clinopyroxenite, SIMAR, siliceous marble; MESD, meta-sandstone.
[b] Pl, plagioclase; Cpx, clinopyroxene; oxd, Fe–Ti oxide.
[c] The $\delta^{18}O$ of magma was calculated from clinopyroxene data assuming $\Delta_{magma-Cpx} = 0.5‰$ (magnetite gabbro) and 0.2‰ (magnetite clinopyroxenite).
[d] Sample consists of ~41% brucite and ~59% calcite.
[e] Sample consists of ~39% brucite and ~61% calcite.
[f] These values are duplicates of each sample.
[g] The $\delta^{18}O$ values of the country rocks are whole rock values.

of clinopyroxene separates from the Middle and Upper Zones of the Hongge intrusion vary from 5.6 to 6.0‰, with an average of 5.8‰ (n = 6). These values are similar to those for the other intrusions (Baima, Panzhihua and Taihe). In contrast, the $\delta^{18}O$ values of clinopyroxene separates from the Lower Zone of the Hongge intrusion are significantly higher, ranging from 6.4 to 6.9‰.

The $\delta^{18}O$ values of plagioclase separates from the Baima and Panzhihua intrusions are highly variable, ranging from 1.8 to 9.7‰, which are significantly different from the calculated value for the hypothetical plagioclase (An_{60}) that may crystallize from the uncontaminated mantle-derived magma with oxygen isotopic composition the same as that of OIB. Similarly, the $\delta^{18}O$ values of Fe–Ti oxide mineral separates from all of the four intrusions (Baima, Hongge, Panzhihua and Taihe) are also highly variable, ranging from −0.7 to +5.5‰; most are lower than the calculated value for the hypothetical Fe–Ti spinel (55% magnetite and 35% ilmenite and 10% ulvöspinel) that may crystallize from an uncontaminated mantle-derived magma with oxygen isotopic composition the same as that of OIB.

5.2. Whole-rock major, trace element and Sr–Nd isotope compositions

The chemical compositions of new rock samples from the Baima intrusion are listed in Table A1. In this intrusion, the $Fe_2O_3^T$ and TiO_2 contents vary from 10.1 to 40.1 wt.% and from 1.75 to 8.21 wt.%, respectively; the abundance of P_2O_5 varies from 0.04 to 0.34 wt.%. New Sr–Nd isotope data of whole-rock samples from the Baima intrusion and the previously-reported Sr–Nd isotope data for the Panzhihua, Taihe, Hongge intrusions (Song et al., 2013; Luan et al., 2014; She et al., 2014) are given in Table A2. The initial $^{87}Sr/^{86}Sr$ ratios and εNd(t) are calculated using the age of 260 Ma, which is similar to the average zircon U–Pb age of these contemporaneous intrusions (Zhou et al., 2005, 2008; Zhong et al., 2011). Based on the limited numbers of analyses for each of the intrusions, no systematic stratigraphic variations in Sr–Nd isotopic compositions are found in these intrusions. The calculated initial $^{87}Sr/^{86}Sr$ ratios and εNd(t) values for all of the four intrusions (Baima, Hongge, Panzhihua and Taihe) range from 0.7043 to 0.7176, and from −3.01 to +2.85, respectively. These values are similar to those for the coeval high-Ti picrites in the ELIP (Fig. 5). Among these intrusions, the Hongge intrusion has the highest initial $^{87}Sr/^{86}Sr$ ratios and lowest εNd(t) values. Other intrusions have similar Sr–Nd isotope compositions.

5.3. Major, trace element and O–Sr–Nd isotope compositions of country rocks

The major and trace element compositions of country rock samples collected from the basal contacts of the Baima, Hongge and Panzhihua intrusions are listed in Table A1. The O–Sr–Nd isotope compositions of these country rocks are listed in Tables 1, and A2. The marbles contain low SiO_2 (0.08–8.72 wt.%) and most trace elements. The contents of Nd and Sm in the marbles are from 0.02 to 1.27 ppm and from 0 to 0.29 ppm, respectively. The other meta-sedimentary country rocks (schist, meta-sandstone and siliceous marble) have higher SiO_2 (43–88.6 wt.%) and most trace elements than the marbles. All of the country rocks are characterized by higher $\delta^{18}O$ values than the coexisting mafic intrusive rocks. The marble and siliceous marble in the footwalls of the Panzhihua and Baima intrusions have $\delta^{18}O$ values ranging from 7.4 to 13.2‰, which is similar the values obtained by

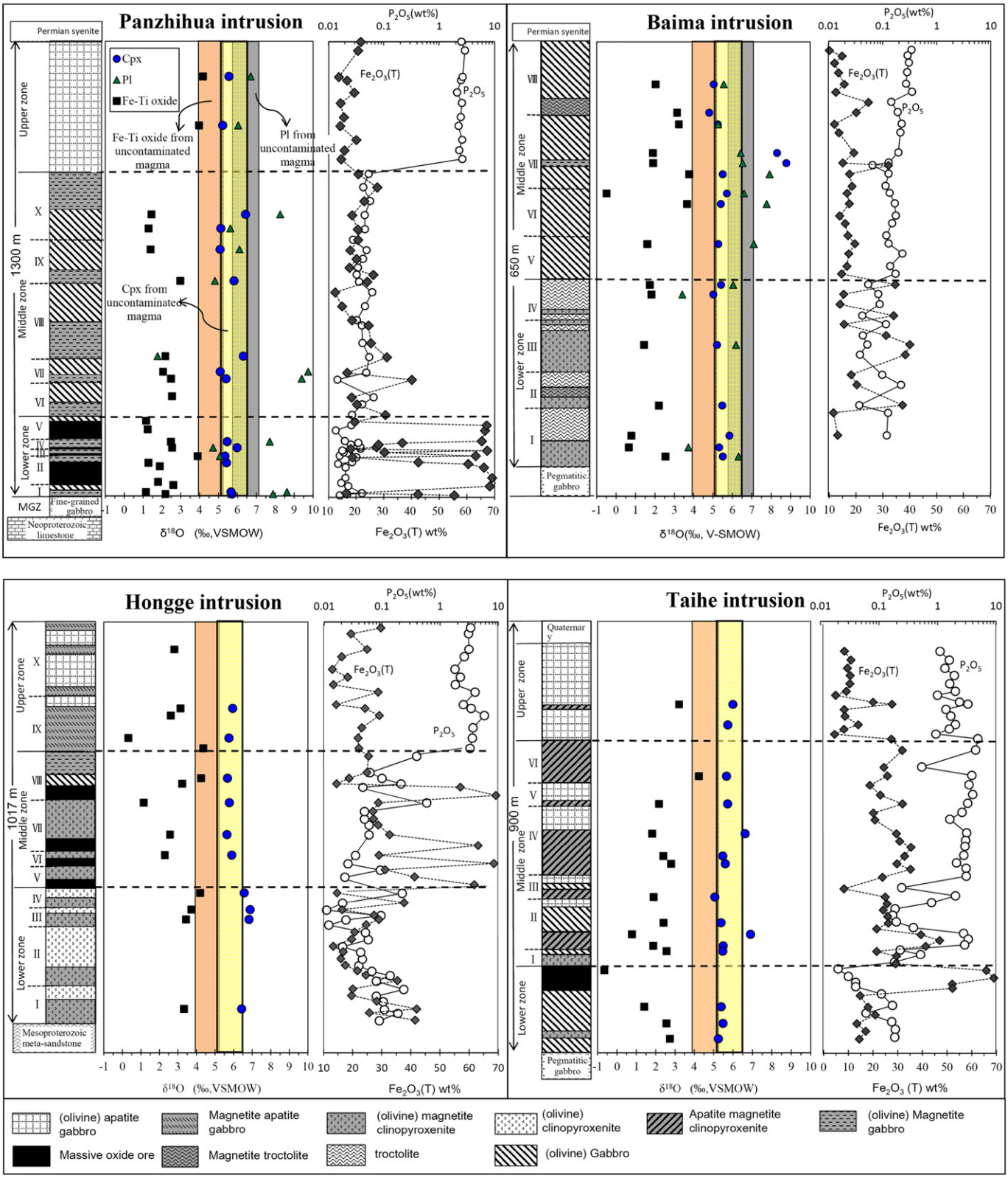

Fig. 4. Stratigraphic variations of mineral $\delta^{18}O$ values (this study) and whole-rock Fe_2O_3(T) and P_2O_5 contents (Song et al., 2013; Luan et al., 2014 and She et al., 2014). The hypothetical values of $\delta^{18}O$ for plagioclase (An_{60}), Fe–Ti oxide (60% magnetite and 40% ilmenite) and clinopyroxene crystallizing from an uncontaminated mantle-derived magma with oxygen isotopic composition the same as that of oceanic island basalt (OIB) are shown as gray, brown and yellow bands, respectively. The hypothetical values are calculated for 1000 °C using the magma–solid fractionation equation of Zhao and Zheng (2003). The OIB value is calculated from the $\delta^{18}O$ value of olivine in OIB from Eiler et al. (1997).

Ganino et al. (2013). Calculated (t = 260 Ma) $^{87}Sr/^{86}Sr$ values ranging from 0.7058 to 0.7078 and calculated (t = 260 Ma) εNd values ranging from −3.05 to −0.78. In comparison, the schists in the footwall of the Panzhihua intrusion have $\delta^{18}O$ values of 7.9 to 11.3‰ and lower calculated (t = 260 Ma) $^{87}Sr/^{86}Sr$ (0.7047 to 0.7054) and higher calculated (t = 260 Ma) εNd (+0.83 to +3.66) than the marbles. The meta-

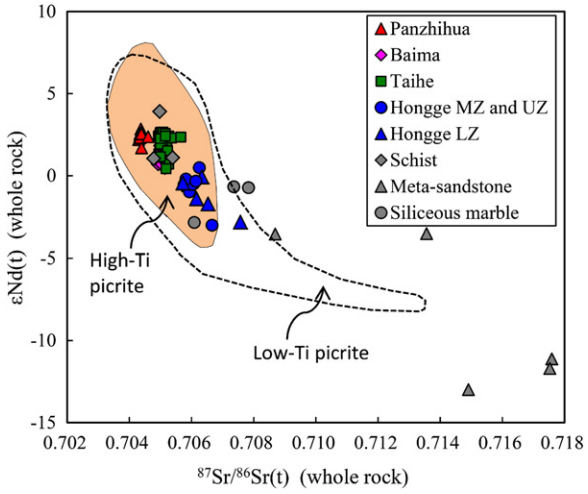

Fig. 5. Plot of εNd values versus initial $^{87}Sr/^{86}Sr$ ratios for the Emeishan large igneous province (T = 260 Ma) and country rocks. The data for the Baima intrusion and country rocks are from this study. The data for other intrusions are from Song et al. (2013), Luan et al. (2014) and She et al. (2014). The data for the volcanic rocks are from Chung and Jahn (1995), Xu et al. (2001), Zhang et al. (2006), Hou et al. (2006), Wang et al. (2007), Hanski et al. (2010), Li et al. (2010), Anh et al. (2011) and Li et al. (2012).

sandstones in the footwalls of the Hongge and Panzhihua intrusions have the highest $\delta^{18}O$ values (11.7 to 17‰), the highest calculated (t = 260 Ma) $^{87}Sr/^{86}Sr$ values (0.7087 to 0.7175) and the lowest calculated (t = 260 Ma) εNd (−13.16 to −3.75).

A comparison of Sr–Nd isotopic compositions between the intrusions and country rocks is illustrated in Fig. 5. The most significant differences are between the meta-sandstone samples from the footwalls of the Hongge and Panzhihua intrusions and the intrusive rocks. The siliceous marbles in the footwall of the Baima intrusion have higher calculated $^{87}Sr/^{86}Sr$ values (t = 260 Ma) and lower calculated (t = 260 Ma) εNd than the Baima intrusive rocks. The schists in the footwall of the Panzhihua intrusion and the Panzhihua intrusive rocks have similar Sr–Nd isotopic compositions.

6. Discussion

The significant differences in O–Sr–Nd isotope compositions between the Fe–Ti oxide ore-bearing mafic–ultramafic intrusions (Baima, Hongge, Panzhihua, and Taihe) in the ELIP and the country rocks can be used to evaluate the role of crustal assimilation in ore genesis. In the following discussion, we will use the $\delta^{18}O$ values of the mineral separates that have been least affected by isotope exchange reactions during subsolidus re-equilibration and post-magmatic hydrothermal alteration to estimate the oxygen isotopic compositions of the parental magmas for the intrusions based on the known mineral–magma oxygen isotope fractionation factors. We use the estimated magma oxygen isotopic composition together with whole-rock Sr–Nd isotopic compositions to evaluate possible crustal contamination and its role in Fe–Ti oxide mineralization in the intrusions.

6.1. Controls on $\delta^{18}O$ variations in minerals

The oxygen isotopic compositions of minerals in mafic–ultramafic rocks mainly depend on (1) oxygen isotopic composition of parental magma, (2) isotope fractionation between melt and minerals during fractional crystallization, (3) subsolidus equilibrium fractionation between coexisting minerals, and (4) open-system isotope exchange between minerals and fluids during post-magmatic fluid–rock interaction.

6.1.1. Oxygen isotope fractionation during fractional crystallization

Fig. 6 illustrates changes in the $\delta^{18}O$ values of mineral and fractionated liquid during fractional crystallization for magma with initial $\delta^{18}O$ value of 6.0‰, which is the same as the average value for OIB (6.0 ± 0.7‰, Eiler et al., 1997). Oxygen isotope fractionation between melt and mineral during fractional crystallization can be estimated using the Rayleigh fractionation equation of $R / R_i = f^{(\alpha - 1)}$ (Rayleigh, 1902). In this equation, R_i and R represent the isotope ratios of initial and residual magma, respectively, f represents percentage of the residual magma, and α represents mineral–magma fractionation factor for oxygen. Per mil difference between mineral and coexisting magma were calculated using the solid–liquid isotopic fractionation equation, $\Delta_{mineral-melt} = A \times 10^6 / T^2$ and the coefficients (A) from Zhao and Zheng, (2003). It is well known that the $\Delta_{mineral-melt}$ values are controlled by temperature and mineral composition (e.g., olivine Fo content and plagioclase An content). In our calculations, we used the mineral compositions and crystallization temperatures of the parental magma for the Panzhihua intrusion from Song et al. (2013) who simulated the fractional crystallization of the magma under the conditions of 1 kbar total pressure and an oxidation state equivalent to the QFM buffer using the MELTS program of Ghiorso and Sack (1995). The modeled results show the following order of ^{18}O-enrichment: plagioclase > apatite > clinopyroxene > olivine > magnetite relative to ilmenite ($\Delta_{magnetite-ilmenite} \leq 0.2‰$). Fractional crystallization of ^{18}O-enriched plagioclase and apatite and ^{18}O-depleted olivine, clinopyroxene and magnetite from 1190 to 1035 °C (85% crystallization) may lead to a progressive increase of $\delta^{18}O$ value in the magma from 6.0 to 6.25‰. The calculated $\delta^{18}O$ values of clinopyroxene, plagioclase and magnetite range from 5.71 to 5.86‰, 6.20 to 6.76‰ and 4.19 to 4.23‰, respectively. The calculated Δ_{Pl-Cpx} and Δ_{Cpx-Mt} values range from 0.54 to 0.90‰ and from 1.3 to 1.55‰, respectively. The calculated results confirm that in basaltic systems fractional crystallization causes only minor shifts in mineral and melt $\delta^{18}O$ values (e.g., Kalamarides, 1984; Dunn, 1986). This also explains why there is no systematic variation of mineral $\delta^{18}O$ values within a single cyclic unit in the layered mafic–ultramafic intrusions of the ELIP that formed by multiple magma replenishments (Zhang et al., 2012; Song et al., 2013; Luan et al., 2014; She et al., 2014). The above results are based on the parental magma composition of the Panzhihua intrusion and may not be accurate for the other three intrusions in the region due to variation in their parental magma compositions.

Most of the samples from the Baima, Hongge, Panzhihua and Taihe intrusions show the following order of the $\delta^{18}O$ values for the coexisting minerals: plagioclase > clinopyroxene > Fe–Ti oxide, which is generally

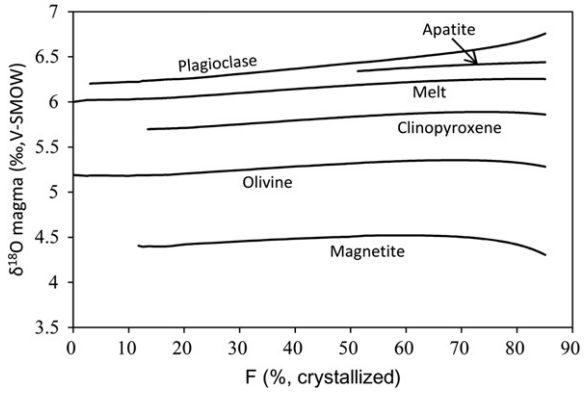

Fig. 6. Modeled changes in $\delta^{18}O$ values for minerals and coexisting liquid as a result of fractional crystallization of a basaltic magma with initial $\delta^{18}O$ value = 6.0‰. The mineral–melt oxygen isotopic fractionation factors from Zhao and Zheng (2003) and the simulated results of temperature variation and compositional changes for minerals during fractional crystallization of a basaltic magma under the conditions of 1 kbar total pressure and an oxidation state equivalent to the QFM buffer given in Song et al. (2013) were used in our calculations.

consistent with the result for cotectic crystallization. In more detail, however, the ranges of the observed Δ_{Pl-Cpx} and Δ_{Cpx-Mt} values for the intrusions ($\Delta_{Pl-Cpx} = -4.6$ to $+4.7$‰, $\Delta_{Cpx-Fe-Ti\ oxide} = 1.4$ to 6.2‰, Table 1) are significantly larger than the predicted values for fractional crystallization ($\Delta_{Pl-Cpx} = 1.8$ to 2.6‰, $\Delta_{Cpx-Mt} = 1.3$ to 1.7‰). This indicates that only small number of samples still preserve the primary $\delta^{18}O$ values for fractional crystallization. The oxygen isotopic compositions for most samples have been affected by subsolidus fractionation between coexisting minerals and post-magmatic hydrothermal alteration. As shown in the plots of $\delta^{18}O_{Cpx}$ versus of $\delta^{18}O_{Fe-Ti\ oxide}$ and $\delta^{18}O_{Pl}$ (Fig. 7a, b), most samples plot below the 1000 °C contour or above the 1200 °C contour. Because the liquidus temperature of a basaltic magma that may represent the parental magma of the intrusions is between 1000 and 1200 °C (Song et al., 2013), the samples that plot below the 1000 °C contour or above the 1200 °C contour must have experienced significant oxygen isotope exchange during subsolidus re-equilibration between minerals or post-magmatic fluid–rock interaction.

Based on textures, some researchers suggested that the massive and semi-massive Fe–Ti oxide layers in the ELIP layered intrusions formed by liquid immiscibility (Wang and Zhou, 2013; Zhou et al., 2013; Liu et al., 2014). This process is evaluated below using the observed variations of oxygen isotope compositions in the selected intrusions. Recent experimental results indicate that ^{18}O slightly favors a Si-rich immiscible melt in contrast to the coexisting Fe-rich melt (Kyser et al., 1998; Lester et al., 2013). The $\Delta^{18}O$ values for the immiscible Si- and Fe-rich melts are from 0.4 to 0.6‰ (Lester et al., 2013), which are significantly smaller than those for coexisting silicate and Fe–Ti oxide minerals crystallizing from basaltic magma. Based on the experimental results, a Fe-rich melt segregated from basaltic magma with $\delta^{18}O$ value similar to that of OIB (6.2 ± 0.7‰) as a result of liquid immiscibility cannot have a $\delta^{18}O$ value lower than 5.6‰, which is much higher than the observed $\delta^{18}O$ values for Fe–Ti oxides from the massive and semi-massive Fe–Ti oxide layers in the ELIP intrusions (up to +5.0‰, Table 1). Clearly, the oxygen isotope data for the oxide ores from this study do not provide evidence for the liquid immiscibility model.

6.1.2. Subsolidus oxygen isotope exchange

Subsolidus fractionation between coexisting minerals in igneous rocks depends on mineral modal compositions and temperature. In the Baima, Hongge, Panzhihua and Taihe intrusions, magnetite gabbro and magnetite clinopyroxenite are two of the most important rock types. The effects of subsolidus oxygen isotope exchange on the $\delta^{18}O$ values of important phases in these two types of rocks are evaluated below.

A typical magnetite gabbro in the ELIP intrusions on average contains 45% plagioclase (An_{60}), 40% clinopyroxene and 15% Fe–Ti oxides (magnetite:ilmenite:ulvöspinel = 55:35:10). Assuming that the $\delta^{18}O$ value of the rock is 5.9‰, which is similar to the value for a Pl + Cpx + Mt cumulate formed after 53% crystallization (at 1130 °C) from a parental magma with $\delta^{18}O$ value of 6.0‰ (Fig. 6), the $\delta^{18}O$ values of clinopyroxene, plagioclase and Fe–Ti oxides at 1130 °C are estimated to be 5.9‰, 6.4‰ and 4.5‰, respectively. The effect of subsolidus isotope exchange between coexisting minerals at a given temperature can be estimated based on oxygen mass balance and isotope fractionation factors. At 750 °C, which is a plausible closure temperature for pyroxene in a medium-grained mafic igneous rocks (Harris, 2005), the Δ_{Cpx-Pl} and $\Delta_{Cpx-Fe-Ti\ oxide}$ are around −1.1‰ and +2.74‰, respectively (Zheng, 1991, 1993). After isotopic exchange at this temperature, the $\delta^{18}O$ values for the coexisting clinopyroxene, plagioclase and Fe–Ti oxide are estimated to be 5.8‰, 6.9‰ and 3.4‰, respectively. Assuming that clinopyroxene does not participate in the isotopic exchange on further cooling down to 550 °C, which is a plausible closure temperature for plagioclase and magnetite (Giletti, 1986; Sharp, 1991), after subsolidus isotope exchange at this temperature, the $\delta^{18}O$ values of plagioclase and coexisting Fe–Ti oxides are estimated to be 7.4‰ and 1.9‰, respectively. During subsolidus re-equilibration at temperatures between 1130 and 550 °C, the calculated $\delta^{18}O$ values for clinopyroxene, plagioclase and Fe–Ti oxide are 5.9–5.8‰, 6.4–7.4‰ and 4.5–1.9‰, respectively. The calculated Δ_{Pl-Cpx} and $\Delta_{Cpx-Fe-Ti\ oxide}$ values are from 0.5 to 1.6‰ and from 1.4 to 3.9‰, respectively. The results show that for the oxide-bearing gabbroic rocks subsolidus equilibrium fractionation between the coexisting minerals has little effect on the $\delta^{18}O$ value of clinopyroxene (~0. 1‰ lower than the initial value) and moderate effect on the $\delta^{18}O$ values of plagioclase and Fe–Ti oxide (1.0‰ higher for plagioclase and 2.6‰ lower for Fe–Ti oxide than the initial values).

A typical magnetite clinopyroxenite in the ELIP intrusions on average contains 85% clinopyroxene and 15% Fe–Ti oxides (magnetite:ilmenite:ulvöspinel = 55:35:10). Assuming that the $\delta^{18}O$ value of this rock is 5.7‰, which is similar to the value for a Cpx–Mt cumulate formed after 53% crystallization (at 1130 °C) from a parental magma with $\delta^{18}O$ value of 6‰ (Fig. 6), our calculations show that at this temperature the $\delta^{18}O$ values of clinopyroxene and Fe–Ti oxides are 5.9‰ and 4.5‰, respectively. After subsolidus isotope exchange at 750 °C, the $\delta^{18}O$ values of clinopyroxene and

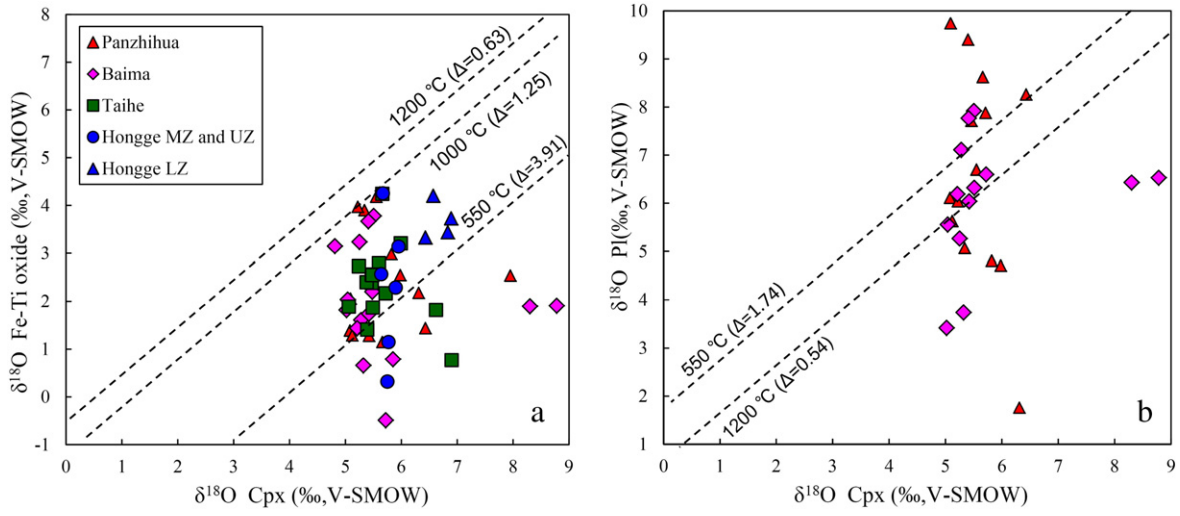

Fig. 7. Plots of the $\delta^{18}O$ values of clinopyroxene versus the $\delta^{18}O$ values of Fe–Ti oxide (a) and plagioclase (b) for several important Fe–Ti oxide ore-bearing mafic–ultramafic intrusions in the ELIP. Per mil difference between clinopyroxene and Fe–Ti oxide ($\Delta_{Cpx-Fe-Ti\ oxide}$) is calculated assuming average Fe–Ti oxide consisting of 55% magnetite + 35% ilmenite + 10% ulvöspinel. In addition, per mil difference between plagioclase and clinopyroxene (Δ_{Pl-Cpx}) is calculated assuming average plagioclase with An value of 60 mol%. Fractionation factors used in our calculation are from Zheng (1991, 1993).

Fe–Ti oxides are estimated to be 6.1‰ and 3.7‰, respectively. After subsolidus re-equilibration, the calculated $\delta^{18}O$ values for clinopyroxene and Fe–Ti oxide are 5.9–6.1‰ and 4.5–3.7‰, respectively. The $\Delta_{Cpx-Fe-Ti\ oxide}$ values vary from 1.4 to 2.4‰. The $\delta^{18}O_{Cpx}$ and $\delta^{18}O_{Fe-Ti\ oxide}$ values for equilibration at 750 °C are only 0.2‰ higher and 0.8‰ lower than those values at 1130 °C, respectively.

Our calculated results demonstrate that the effect of subsolidus equilibrium fractionation on clinopyroxene is similarly insignificant for both types of rocks, which is consistent with the relatively limited variation of $\delta^{18}O$ (5–7‰) values for clinopyroxene in most samples from the Baima, Hongge, Panzhihua and Taihe intrusions. The modeled results also show that subsolidus isotope exchange between minerals can cause more significant changes in $\delta^{18}O$ values for both plagioclase and Fe–Ti oxide. The observed ranges of $\delta^{18}O$ values for plagioclase (1.8 to 9.7‰) and Fe–Ti oxide (−0.7 to 5‰) from the ELIP intrusions are much larger than the predicted values for subsolidus equilibrium fractionation alone. Similarly, the observed ranges of Δ_{Pl-Cpx} (−4.6 to 4.7‰) and Δ_{Cpx-Mt} (1.4 to 6.2‰) values for the Baima, Hongge, Panzhihua and Taihe intrusions are also significantly larger than the predicted values for subsolidus equilibrium fractionation alone. Such inconsistencies are clearly shown in the plots of $\delta^{18}O_{Cpx}$ versus $\delta^{18}O_{Fe-Ti\ oxide}$ and $\delta^{18}O_{Pl}$ (Fig. 7a, b), in which a large amount of samples show disequilibrium oxygen isotopic signatures between coexisting mineral pairs. This can be attributed to hydrothermal overprinting. This process has affected plagioclase and Fe–Ti oxide more than coexisting clinopyroxene, resulting in significant displacements of the observed values from the predicted values for equilibrium isotope exchange at low temperatures.

6.1.3. Rock–fluid interaction

Geologic evidence indicates that the areas of most intense saussuritization and chloritization are found within a more highly fractured zone of drill core. The ^{18}O enrichment of plagioclase is commonly accompanied by variable degrees of saussuritization, such as samples SP05-3 and SP05-42. Some massive and semi-massive oxide ores such as samples SP05-3 and SP05-42 that are fractured and highly altered (Fig. 3d) have extremely low $\delta^{18}O$ values (<2.5‰). Because the $\delta^{18}O$ values of plagioclase and Fe–Ti oxide change more rapidly with time than clinopyroxene (Gregory and Taylor, 1981; Ripley et al., 2008), differential rates of exchange between any fluid and minerals will result in steep, negative or positive-sloped arrays on the plots of $\delta^{18}O_{Cpx}$ versus $\delta^{18}O_{Fe-Ti\ oxide}$ and $\delta^{18}O_{Pl}$ (Fig. 7). Oxygen isotope exchange at elevated temperatures (400°–500 °C) with an assumed low-^{18}O fluid (−10‰), which is similar to the $\delta^{18}O$ values of modern meteoric water, will cause progressive ^{18}O depletion for both plagioclase and Fe–Ti oxide. Some samples from the Baima and Panzhihua intrusions show unusually low $\delta^{18}O$ values for both plagioclase and Fe–Ti oxide separates (Fig. 7b). This can be attributed to interaction of these minerals with low-^{18}O fluid at elevated temperatures (> ~ 400 °C). Taking the lowest plagioclase $\delta^{18}O$ value of 1.8‰ (SP05-28) as an extreme example, the calculated $\delta^{18}O$ value of water which equilibrated with plagioclase in this sample at 450 °C is close to +0.9‰ using the fractionation factor of Zheng (1993). If such evolved, ^{18}O enriched fluid recirculates into the intrusion when the intrusion cools down to 150°–200 °C, subsequent oxygen isotope exchange will cause ^{18}O enrichment for plagioclase but depletion for Fe–Ti oxide. Some samples from the Baima and Panzhihua intrusions show unusually high $\delta^{18}O$ values (>7.5‰) for plagioclase separates and unusually low $\delta^{18}O$ values (<3‰) for Fe–Ti oxide separates (Fig. 7a, b). This is consistent with interaction with the evolved, ^{18}O enriched meteoric water at low temperatures. Alternatively, the highly variable $\delta^{18}O$ values of plagioclase and Fe–Ti oxide can also be attributed to isotope exchange with hydrothermal fluids that have multiple sources, such as metamorphic fluid, meteoric water or seawater. This scenario needs to be further evaluated using combined oxygen and hydrogen isotope determination. In most of the samples, clinopyroxene still retains a normal range of $\delta^{18}O$ values (5–6‰). This is because clinopyroxene is much less susceptible to fluid modification than plagioclase and Fe–Ti oxide (e.g., Taylor, 1967; Gregory and Taylor, 1981).

6.2. Estimation of parental magma $\delta^{18}O$ values

Because clinopyroxene is much less susceptible to oxygen isotope exchange during subsolidus re-equilibration and post-magmatic hydrothermal alteration than coexisting plagioclase and Fe–Ti oxides, we have used the observed oxygen isotope compositions of clinopyroxene separates from the Baima, Hongge, Panzhihua and Taihe intrusions to estimate the oxygen isotope compositions of the parental magmas. In our calculations the effects of sub-solidus oxygen isotope exchange on clinopyroxene oxygen isotope compositions were corrected by adding +0.2‰ and −0.1‰ to the observed $\delta^{18}O$ values of clinopyroxene separates from the gabbros and clinopyroxenites, respectively. As described above, these two correction factors are based on the modeled results for a magnetite gabbro and a magnetite clinopyroxenite, respectively. The corrected $\delta^{18}O$ values of clinopyroxene separates were then used to estimate the $\delta^{18}O$ values of the parental magmas using the $\Delta_{melt-Cpx}$ of 0.3, which is the value for the equilibration temperature of 1200 °C (Zhao and Zheng, 2003). The estimated $\delta^{18}O$ values for the parental magmas of the samples from the Baima, Hongge, Panzhihua and Taihe intrusions are given in Table 1. Except three samples which give anomalously high $\delta^{18}O_{melt}$ value of 6.8, 6.9 and 8.5‰, the rest of the samples from the Panzihua intrusion give a small range of $\delta^{18}O_{melt}$ values from 5.6 to 6.5‰ (mean value 6.0‰, n = 13). Excluding two samples with anomalously high $\delta^{18}O_{melt}$ values (8.8‰ and 9.3‰), the estimated $\delta^{18}O_{melt}$ values for the Baima intrusion are from 5.2 to 6.2‰ (mean value 5.7‰; n = 14). Excluding two anomalously high values (6.8 and 7.0‰), the estimated $\delta^{18}O_{melt}$ values for the Taihe intrusion are between 5.3‰ and 6.2‰ (mean value 5.9‰; n = 13). The estimated $\delta^{18}O_{melt}$ values for the Upper and Middle Zones of the Hongge intrusion vary from 5.8 to 6.5‰ (mean value 6.2‰; n = 6), similar to the normal ranges for the other three intrusions (Baima, Panzhihua and Taihe). It is interesting that the mean estimated $\delta^{18}O_{melt}$ values for the Upper and Middle Zones of the Hongge intrusion, as well as for the other three contemporaneous intrusions in the ELIP, are remarkably similar to that of uncontaminated magma and those for the Kiglapait, Stillwater and Freetown mafic–ultramafic intrusions elsewhere in the world (Table A3) (Kalamarides, 1984; Dunn, 1986; Chalokwu et al., 1999). The estimated $\delta^{18}O_{melt}$ values for the Lower Zone of the Hongge intrusion (6.6 to 7.1‰ with a mean of 6.9‰, n = 4) are higher than those for the Upper and Middle Zones of the Hongge intrusion but similar to those for the Bushveld Complex in South Africa and the Great Dyke in Zimbabwe (Table A3) (Chaumba and Wilson, 1997; Harris, 2005).

6.3. Constraints on crustal contamination

Previous studies have shown that in the Emeishan large igneous province picrites are the most primitive and least contaminated by crustal materials (Zhang et al., 2006; Wang et al., 2007; Hanski et al., 2010; Li et al., 2010, 2012). As shown in Fig. 5, the Sr–Nd isotope compositions of the Panzhihua, Baima and Taihe intrusions are similar to those of the Emeishan high-Ti picrites, indicating no significant crustal contamination in these intrusions. This is further supported by the mantle-like $\delta^{18}O_{melt}$ values (mean values: Panzhihua, 6.1‰, Baima, 5.7‰, Taihe, 5.9‰) (Table A3). The $^{87}Sr/^{86}Sr_i$ and εNd_t values of the Hongge intrusion are also within the ranges of the Emeishan high-Ti picrites, but show more radiogenic signatures than the other three intrusions (Fig. 5). As described above, the estimated $\delta^{18}O_{melt}$ values for the Upper and Middle Zones of the Hongge intrusion are similar to those for the other three intrusions, but these values for the Lower Zone of the Hongge intrusion are slightly higher. This observation, together with more radiogenic Sr–Nd isotopic signatures in this zone, indicates more significant crustal contamination in this part of the intrusion.

The variations in degree of crustal contamination in the selected Fe–Ti oxide ore-bearing intrusions in the ELIP may be evaluated by mixing calculations using O–Sr–Nd isotopes. The results of our calculations are illustrated in Fig. 8. The samples from the Baima, Panzhihua and Taihe intrusions plot close to the center of the OIB field. The samples from the Hongge intrusion, particularly those from its Lower Zone plot slightly away from the center of the OIB field. The differences between the Hongge intrusion and the other intrusions can be explained by up to 12% more crustal contamination in the former than the later. The O–Sr–Nd isotopic data reveal that among the different types of country rocks in the region, the meta-sandstone is the most important contaminant (Fig. 8). Dolomite and marble country rocks plot far away from the mixing lines due to extremely high $\delta^{18}O$ values (7–28‰, Table 1 and Ganino et al., 2013). This indicates that bulk assimilation of the carbonates is negligible for these intrusions. We use the average $\delta^{18}O$ value of OIB (6‰, Eiler et al., 1997) and the Sr–Nd isotope compositions of an uncontaminated Emeishan picrite (EM–83 ($^{87}Sr/^{86}Sr)_i = 0.70458$; $\varepsilon Nd_t =$ 2.8; Sr = 148 ppm; Nd = 19.43 ppm, Chung and Jahn (1995)) to represent the composition of the uncontaminated mantle-derived magma. The country rock marbles are unlikely to be the possible contaminants involved because these rocks have low Sr and Nd contents (Sr = 37–96.4 ppm; Nd = 0–1.27 ppm, Table A1). In contrast, the meta-sandstones display relatively high Sr and Nd concentrations (Sr = 111–237 ppm; Nd = 9.75–92.74 ppm) and they are better choices to be used as possible contaminants in the mixing calculation. Therefore, we use the O–Sr–Nd isotopic compositions of a meta-sandstone sample from the footwall of the Hongge intrusion (SH10-40 ($^{87}Sr/^{86}Sr)_i =$ 0.717588; $\varepsilon Nd_t = -11.12$; $\delta^{18}O = 17.03‰$; Sr = 237 ppm; Nd = 92.7 ppm) to represent the composition of the possible contaminant. The results of simple mixing calculations show that <5% of crustal contamination is required to explain the observed isotopic composition of the Baima, Panzhihua and Taihe intrusions. Up to 10% of crustal contamination is required to explain the isotopic compositions of the Middle and Upper Zones of the Hongge intrusion. The Lower Zone of the Hongge intrusion appears to have experienced the highest degrees of crustal contamination, up to 15% (Fig. 8). These percentages are maximum values and may be reduced if contamination was selective in nature, involving Sr- and Nd-bearing fluids or partial melts.

6.4. The role of CO_2 in ore formation

Thick massive to semi-massive Fe–Ti oxide layers (up to 60 m) occur in the Lower Zone of the Panzhihua intrusion which intruded Proterozoic dolomites. Ganino et al. (2008) proposed the oxide ore formation in

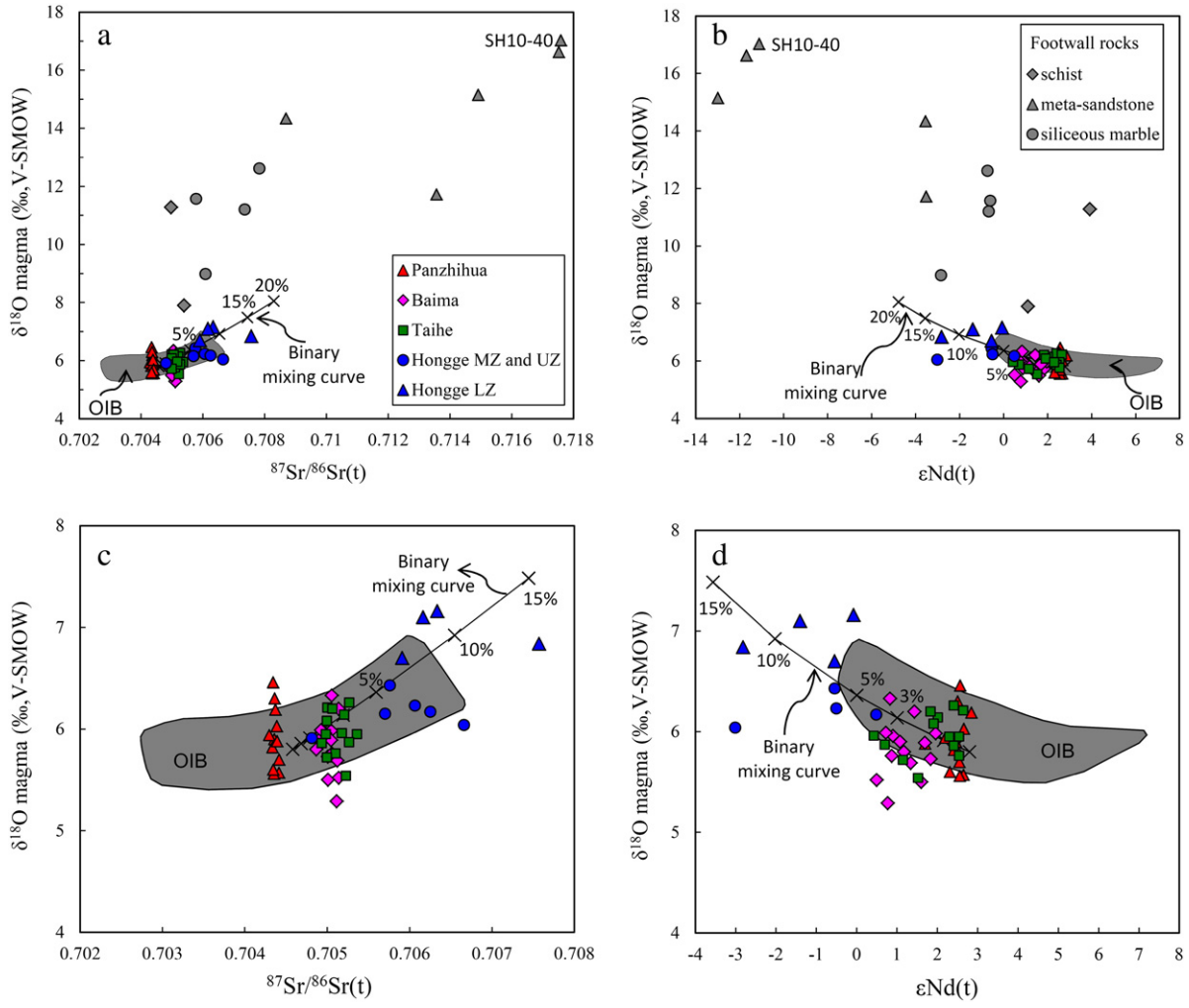

Fig. 8. Plots of estimated $\delta^{18}O$ values for the parental magmas of several important Fe–Ti oxide ore-bearing mafic–ultramafic intrusions in the ELIP and their whole-rock Sr–Nd isotopic compositions (a, b), the footwall rocks are included for comparison. Enlarged plots of $\delta^{18}O$ values for the parental magmas of ELIP intrusions and their Sr–Nd isotopic compositions (c, d) are also shown. The binary mixing lines in black color were calculated using a picritic basalt in the ELIP from Chung and Jahn (1995) (EM-83: $^{87}Sr/^{86}Sr(i) = 0.70458$; $\varepsilon Nd(t) =$ 2.8; Sr = 148 ppm; Nd = 19.43 ppm) and a meta-sandstone footwall rock sample (SH10-40: $^{87}Sr/^{86}Sr(i) = 0.717588$; $\varepsilon Nd(t) = -11.12$; $\delta^{18}O = 17.03‰$, Sr = 237 ppm; Nd = 92.7 ppm). The $\delta^{18}O$ value for EM-83 is assumed to be 5.8‰. The range of $\delta^{18}O$ values for ocean island basalts (OIB) were calculated from the oxygen isotopic compositions of olivine phenocrysts (Eiler et al., 1997) using the olivine–liquid fractionation equation of Zhao and Zheng (2003).

the intrusion is due to oxidation of magma by infiltration of CO_2 released from footwall carbonates during contact metamorphism. They envisioned that if the decarbonation process and fluid infiltration happened simultaneously, dolomite would react with water to produce calcite and brucite via the following reaction:

$$CaMg(CO_3)_2(dol) + H_2O = CaCO_3(cal) + Mg(OH)_2(brucite) + CO_2. \quad (1)$$

At shallow depth (<3 km), the breakdown of dolomite via the above equation will proceed at >400 °C (Turner, 1965). Because ^{18}O is enriched in CO_2 over the coexisting solids during decarbonation (Valley, 1986), the $\delta^{18}O$ values of the residual rocks will be lower than the protoliths. Volatilization of CO_2 in metamorphic rocks commonly results in a modest decrease in $\delta^{18}O$ values of residual rocks (Valley, 1986). In most cases marble in contact aureoles typically show a greater decrease in $\delta^{18}O$ values than can be explained by volatilization of CO_2 (Bowman et al., 1994; Ferry et al., 2002). Substantial $\delta^{18}O$ depletions require infiltration of low-^{18}O magmatic fluid or hydrothermal fluid (Bowman et al., 1994). Fluid infiltration also occurred in the Panzhihua footwall carbonates during contact metamorphism (Ganino et al., 2013). The infiltrated fluid in the Panzhihua contact aureole was unlikely to have been of magmatic origin because the parental magma of the Panzhihua intrusion is considered to have been poor in water (Pang et al., 2008). We speculate that the fluid which infiltrated the aureole was meteoric water within the country rocks that was convecting due to the heat associated with the magmatic activity.

In the following calculation of the $\delta^{18}O$ value for released CO_2 during contact metamorphism, both decarbonation and fluid infiltration processes are considered. Oxygen isotope fractionation during the above reaction process (reaction (1)) can be simulated using an iterative calculation using oxygen mass balance and isotope fractionation factors. The initial $\delta^{18}O$ value for the dolomite is assumed to be 25‰ according to the mean value of regional Proterozoic limestone and dolomite (Ganino et al., 2013). The $\delta^{18}O$ value for the infiltrated fluid is assumed to be −8‰ (higher values produce even more elevated calcite $\delta^{18}O$ values — see below), which is similar to the $\delta^{18}O$ values of modern meteoric water in this region. The amount of infiltrating fluid in each increment is governed by rock porosity. We use a constant rock porosity of ~0.2% in our iterative calculation. The time-integrated water/rock ratio increases gradually with continuous fluid infiltration during decarbonation. The produced CO_2 in each increment is assumed to be in equilibrium with produced calcite temporarily until pressure (e.g., fluid infiltration) becomes sufficient to force the CO_2 out of the area. In addition, we use $\Delta_{CO2-calcite}$ of 7.6‰ and $\Delta_{calcite-brucite}$ of 7.76‰ at 400 °C from Zheng (1990) in the calculation of $\delta^{18}O$ values for produced CO_2 and calcite. Using these parameters the results of an iterative calculation are illustrated in Fig. 9. The calculated results demonstrate that the $\delta^{18}O$ values for produced calcite decrease from 24.6 to 22.3‰ as a function of time-integrated water/rock ratio. The calculated $\delta^{18}O$ values for calcite are higher than the observed values in the Panzhihua marbles (from 12.9 to 19.6‰, Ganino et al., 2013). The difference indicates that the simple calcite–brucite producing reaction with decarbonation cannot give as low of calcite $\delta^{18}O$ values as those observed. Thus, the observed low $\delta^{18}O$ values for the Panzhihua calcite can be attributed to continued isotope exchange between infiltrating fluid and produced calcite after the decarbonation process. On the other hand, the calculated results demonstrate that the $\delta^{18}O$ values for produced CO_2 decrease from 32.2 to 29.9‰ (mean value 31‰) as a function of time-integrated water/rock ratio (Fig. 9).

Hence a mean value of 31‰ for the released CO_2 is used in the following modeling of CO_2 infiltration through magma. If such CO_2-rich fluids passed through the Panzhihua magma chamber, oxygen isotope exchange between magma and CO_2 would take place efficiently because of high (>1000 °C) temperatures. Oxygen isotope fractionation between a passing aliquot of CO_2 and magma can be calculated using a mass conservation equation of the type: $C\ \delta^{i}_{CO2} + M\ \delta^{i}_{magma} = C\ \delta^{f}_{CO2} + M\ \delta^{f}_{magma}$, in which i is initial value, f is final value after exchange, C is at.% of CO_2 oxygen in the total system, and M is at.% of exchangeable magma oxygen in the total system. At 1200 °C, the $\Delta_{CO2-magma}$ is estimated to be 3.2 using the fractionation factors given by Richet et al. (1977). Using these parameters, the result of an iterative calculation with a CO_2/magma mass ratio = 1/1000 for each increment is illustrated in Fig. 10. To change the $\delta^{18}O$ value of a magma from 5.8‰ to 6‰ in this way, the cumulative amount of the transient CO_2 is ~0.5 wt.% based on our calculations (Fig. 10). This value is one order of magnitude less than the amount that is required to oxidize the magma sufficiently to cause the crystallization of Fe–Ti oxides only (Ganino et al., 2008). Hence, we do not believe that footwall decarbonation played a major role in the formation of Fe–Ti–V oxide ores in the Panzhihua intrusion.

As discussed above, the Panzhihua magma reacted with only ~0.5 wt.% of CO_2 released from the footwall during contact metamorphism. On the other hand, minor crustal contamination (<5%) by siliceous materials would only change the $\delta^{18}O$ value of the Panzhihua magma from 5.8‰ to 5.86‰ (see Section 6.3). It is difficult to differentiate these two processes based only on the oxygen isotope signature of the Panzhihua intrusion. It is possible that both crustal contamination involving siliceous rock types and the addition of CO_2 contributed to the oxygen isotope signature of the Panzhihua intrusion if the effects

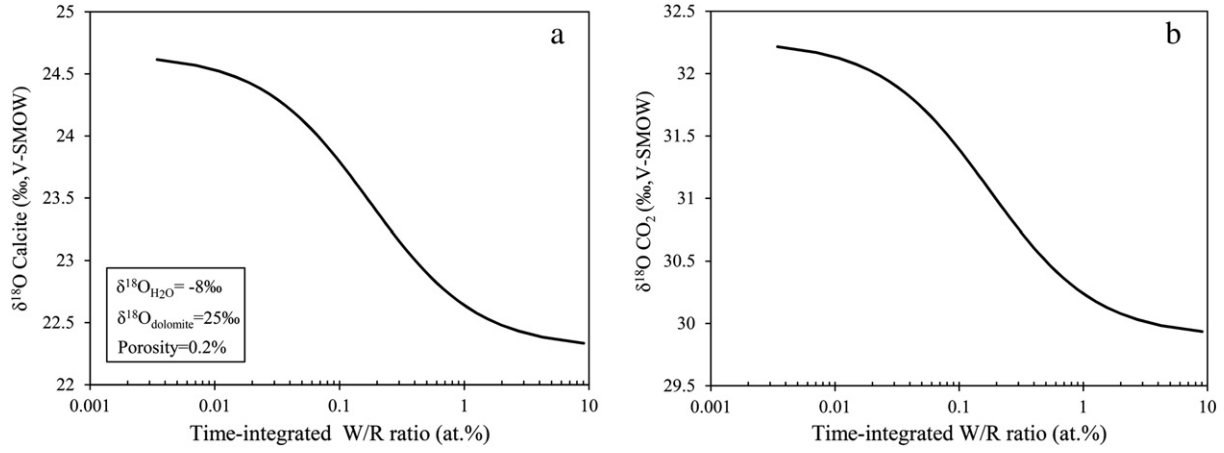

Fig. 9. Changes of $\delta^{18}O$ values in the produced calcite (a) and CO_2 (b) as a function of time-integrated water/rock ratio during the decarbonation and fluid infiltration processes. The $\delta^{18}O$ values for starting dolomite and infiltrating fluid are assumed to be 25‰ and −8‰, respectively. An estimated porosity of 0.2% is used in the iterative calculation.

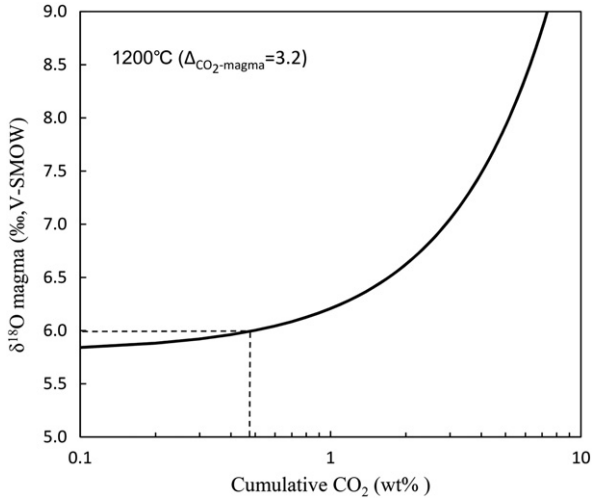

Fig. 10. Change of δ^{18}O value in magma as a function of cumulative CO_2 passing through the magma. The initial δ^{18}O values for the magma and CO_2 are 5.8‰ and 31‰, respectively. The CO_2/magma mass ratio for each increment in the iterative calculation is 1/1000.

of both these sources were small. However, such small amounts of siliceous crustal contamination or CO_2 addition could have played only a minor role in the formation of the Fe–Ti oxide ore layers in the ELIP intrusions as discussed above. More recently, some researchers (e.g., Song et al., 2013; Luan et al., 2014; She et al., 2014) proposed that the Fe–Ti oxide ore-bearing intrusions in the ELIP formed by multiple replenishments of Fe–Ti-enriched magma that was generated by extensive fractional crystallization of olivine and pyroxene in the staging chambers. They believed that this magma was saturated with Fe–Ti oxides during ascent or upon emplacement, and that the ore layers formed by gravitational settling of Fe–Ti oxide crystals from the flow-through magma. The O–Sr–Nd isotopic data reported above is consistent with this alternative model.

7. Conclusions

Our results show that the δ^{18}O values of clinopyroxene from the ELIP intrusions vary narrowly from 5.0 to 6.9‰ due to lack of significant subsolidus oxygen isotope exchange with other coexisting phases and post-magmatic fluids. In contrast, the δ^{18}O values of coexisting plagioclase and Fe–Ti oxide vary widely from 1.8 to 9.7‰ and from −0.7 to +5.5‰, respectively, possibly due to pervasive subsolidus oxygen isotope exchange between coexisting minerals plus post-magmatic hydrothermal overprinting. The oxygen isotope data of clinopyroxene are more useful than those of coexisting plagioclase and Fe–Ti oxide for the study of primary magmatic processes. The combination of clinopyroxene oxygen isotope data and whole-rock Sr–Nd isotopes indicate that the Baima, Taihe and Panzhihua intrusions experienced <5% bulk crustal contamination by siliceous materials. Mixing calculations show that the Hongge intrusion experienced up to 10% crustal contamination in the Upper and Middle Zones and up to 15% in the Lower Zone, and that the other intrusions experienced slightly less degrees of contamination. The estimated percentages of contamination based on the isotope data will be lower if the contamination was selective, involving Sr- and Nd-bearing fluids or partial melts. We found no evidence for significant bulk assimilation of dolomite country rocks in these intrusions. Addition of CO_2 that was released from the country rocks by decarbonation to the magmas of these intrusions could have played only a minor role in the formation of the Fe–Ti oxide ore layers in the ELIP layered intrusions.

Supplementary data to this article can be found online at http://dx.doi.org/10.1016/j.chemgeo.2015.02.020.

Acknowledgments

We thank Benjamin S. Underwood and Jim Brophy for their kind help with sample preparation and oxygen isotope analysis at the Indiana University. This study was funded by the CAS/SAFEA International Partnership Program for Creative Research Teams (KZZD-EW-TZ-20), the National Basic Research Program of China (2012CB416804) and research grants from the State Key Laboratory of Ore Deposit Geochemistry (SKLODG-ZY125-06) and NSFC (40730420, 41373042 and 41473024). We greatly appreciate Professor Chris Harris and an anonymous reviewer for their constructive reviews and Dr. Catherine Chauvel for diligent editorial handling.

References

Ali, J.R., Thompson, G.M., Song, X., Wang, Y., 2002. Emeishan basalts (SW China) and the 'end-Guadalupian' crisis: magnetobiostratigraphic constraints. J. Geol. Soc. 159, 21–29.
Anh, T.V., Pang, K.-N., Chung, S.-L., Lin, H.-M., Hoa, T.T., Anh, T.T., Yang, H.-J., 2011. The Song Da magmatic suite revisited: a petrologic, geochemical and Sr–Nd isotopic study on picrites, flood basalts and silicic volcanic rocks. J. Asian Earth Sci. 42, 1341–1355.
Bai, Z.-J., Zhong, H., Naldrett, A.J., Zhu, W.-G., Xu, G.-W., 2012. Whole-rock and mineral composition constraints on the genesis of the giant Hongge Fe–Ti–V oxide deposit in the Emeishan large igneous province, Southwest China. Econ. Geol. 107, 507–524.
Bouvier, A., Vervoort, J.D., Patchett, P.J., 2008. The Lu–Hf and Sm–Nd isotopic composition of CHUR: constraints from unequilibrated chondrites and implications for the bulk composition of terrestrial planets. Earth Planet. Sci. Lett. 273, 48–57.
Bowman, J.R., Willett, S.D., Cook, S.J., 1994. Oxygen isotopic transport and exchange during fluid flow: one-dimensional models and applications. Am. J. Sci. 294, 1–55.
Chalokwu, C.I., Ripley, E.M., Park, Y.-R., 1999. Oxygen isotopic systematics of an open-system magma chamber: an example from the Freetown Layered Complex of Sierra Leone. Geochim. Cosmochim. Acta 63, 675–685.
Chaumba, J.B., Wilson, A.H., 1997. An oxygen isotope study of the Lower Mafic Succession of the Darwendale Subchamber of the Great Dyke Zimbabwe. Chem. Geol. 135, 293–305.
Chung, S.-L., Jahn, B.-M., 1995. Plume–lithosphere interaction in generation of the Emeishan flood basalts at the Permian–Triassic boundary. Geology 23, 889–892.
Clayton, R.N., Mayeda, T.K., 1963. The use of bromine pentafluoride in the extraction of oxygen from oxides and silicates for isotopic analysis. Geochim. Cosmochim. Acta 27, 43–52.
Dunn, T., 1986. An investigation of the oxygen isotope geochemistry of the stillwater complex. J. Petrol. 27, 987–997.
Eiler, J.M., Farley, K.A., Valley, J.W., Hauri, E., Craig, H., Hart, S.R., Stolper, E.M., 1997. Oxygen isotope variations in ocean island basalt phenocrysts. Geochim. Cosmochim. Acta 61, 2281–2293.
Ferry, J.M., Wing, B.A., Penniston-Dorland, S.C., Rumble, D., 2002. The direction of fluid flow during contact metamorphism of siliceous carbonate rocks: new data for the Monzoni and Predazzo aureoles, northern Italy, and a global review. Contrib. Mineral. Petrol. 142, 679–699.
Ganino, C., Arndt, N., Zhou, M.-F., Gaillard, F., Chauvel, C., 2008. Interaction of magma with sedimentary wall rock and magnetite ore genesis in the Panzhihua mafic intrusion SW China. Mineral. Deposita 43, 677–694.
Ganino, C., Harris, C., Arndt, N.T., Prevec, S.A., Howarth, G.H., 2013. Assimilation of carbonate country rock by the parent magma of the Panzhihua Fe–Ti–V deposit (SW China): evidence from stable isotopes. Geosci. Front. 4, 547–554.
Ghiorso, M.S., Sack, R.O., 1995. Chemical mass transfer in magmatic processes IV. A revised and internally consistent thermodynamic model for the interpolation and extrapolation of liquid–solid equilibria in magmatic systems at elevated temperatures and pressures. Contrib. Mineral. Petrol. 119, 197–212.
Giletti, B.J., 1986. Diffusion effects on oxygen isotope temperatures of slowly cooled igneous and metamorphic rocks. Earth Planet. Sci. Lett. 77, 218–228.
Govindaraju, K., 1994. 1994 compilation of working values and sample description for 383 geostandards. Geostand. Newslett. 18, 1–158 (special issue).
Gregory, R.T., Taylor, H.P., 1981. An oxygen isotope profile in a section of Cretaceous oceanic crust, Samail Ophiolite, Oman: evidence for δ^{18}O buffering of the oceans by deep (>5 km) seawater-hydrothermal circulation at mid-ocean ridges. J. Geophys. Res. 86, 2737–2755.
Hanski, E., Kamenetsky, V.S., Luo, Z.-Y., Xu, Y.-G., Kuzmin, D.V., 2010. Primitive magmas in the Emeishan Large Igneous Province, southwestern China and northern Vietnam. Lithos 119, 75–90.
Harris, C., 2005. Oxygen and hydrogen isotope stratigraphy of the Rustenburg Layered Suite, Bushveld Complex: constraints on crustal contamination. J. Petrol. 46, 579–601.
Hou, Z., Lu, J., Lin, S., 2006. Heterogeneity of a plume axis: bulk-rock geochemical evidence from picrites and basalts in the Emei large igneous province, Southwest China. Int. Geol. Rev. 48, 1087–1112.
Kalamarides, R.I., 1984. Kiglapait geochemistry VI: oxygen isotopes. Geochim. Cosmochim. Acta 48, 1827–1836.
Kyser, T., Lesher, C., Walker, D., 1998. The effects of liquid immiscibility and thermal diffusion on oxygen isotopes in silicate liquids. Contrib. Mineral. Petrol. 133, 373–381.
Lester, G.W., Kyser, T.K., Clark, A.H., 2013. Oxygen isotope partitioning between immiscible silicate melts with H_2O P and S. Geochim. Cosmochim. Acta 109, 306–311.

Li, J., Xu, J.-F., Suzuki, K., He, B., Xu, Y.-G., Ren, Z.-Y., 2010. Os, Nd and Sr isotope and trace element geochemistry of the Muli picrites: insights into the mantle source of the Emeishan large igneous province. Lithos 119, 108–122.
Li, C., Tao, Y., Qi, L., Ripley, E.M., 2012. Controls on PGE fractionation in the Emeishan picrites and basalts: constraints from integrated lithophile–siderophile elements and Sr–Nd isotopes. Geochim. Cosmochim. Acta 90, 12–32.
Liu, H.Y., 1991. Sinian Strata in China. Scientific Press, Beijing (in Chinese).
Liu, P.-P., Zhou, M.-F., Chen, W.T., Boone, M., Cnudde, V., 2014. Using multiphase solid inclusions to constrain the origin of the Baima Fe–Ti–(V) oxide deposit, SW China. J. Petrol. 55, 951–976.
Luan, Y., Song, X.-Y., Chen, L.-M., Zheng, W.-Q., Zhang, X.-Q., Yu, S.-Y., She, Y.-W., Tian, X.-L., Ran, Q.-Y., 2014. Key factors controlling the accumulation of the Fe–Ti oxides in the Hongge layered intrusion in the Emeishan large igneous province SW China. Ore Geol. Rev. 57, 518–538.
McArthur, J., 1994. Recent trends in strontium isotope stratigraphy. Terra Nova 6, 331–358.
McBirney, A.R., 1989. The Skaergaard layered series: I. Structure and average compositions. J. Petrol. 30, 363–397.
Pang, K.-N., Zhou, M.-F., Lindsley, D., Zhao, D., Malpas, J., 2008. Origin of Fe–Ti oxide ores in mafic intrusions: evidence from the Panzhihua intrusion, SW China. J. Petrol. 49, 295–313.
Pang, K.-N., Li, C., Zhou, M.-F., Ripley, E.M., 2009. Mineral compositional constraints on petrogenesis and oxide ore genesis of the late Permian Panzhihua layered gabbroic intrusion, SW China. Lithos 110, 199–214.
Panxi Geological Unit, 1984. Mineralization and exploration forecasting of V–Ti magnetite deposits in the Panzhihua–Xichang Region (in Chinese).
Qi, L., Hu, J., Gregoire, D.C., 2000. Determination of trace elements in granites by inductively coupled plasma mass spectrometry. Talanta 51, 507–513.
Rayleigh, L., 1902. On the distillation of binary mixtures. Philos. Mag. 4, 521–537.
Reynolds, I.M., 1985. The nature and origin of titaniferous magnetite-rich layers in the upper zone of the Bushveld Complex; a review and synthesis. Econ. Geol. 80, 1089–1108.
Richet, P., Bottinga, Y., Javoy, M., 1977. A review of hydrogen, carbon, oxygen, sulfur and chlorine isotope fractionation among gaceous molecules. Annu. Rev. Earth Planet. Sci. 5, 65–110.
Ripley, E.M., Shafer, P., Li, C., Hauck, S.A., 2008. Re–Os and O isotopic variations in magnetite from the contact zone of the Duluth Complex and the Biwabik Iron Formation, northeastern Minnesota. Chem. Geol. 249, 213–226.
Sharp, Z., 1991. Determination of oxygen diffusion rates in magnetite from natural isotopic variations. Geology 19, 653–656.
She, Y.-W., Yu, S.-Y., Song, X.-Y., Chen, L.-M., Zheng, W.-Q., Luan, Y., 2014. The formation of P-rich Fe–Ti oxide ore layers in the Taihe layered intrusion SW China: implications for magma-plumbing system process. Ore Geol. Rev. 57, 539–559.
Song, X.-Y., Zhou, M.-F., Hou, Z.-Q., Cao, Z.-M., Wang, Y.-L., Li, Y., 2001. Geochemical constraints on the mantle source of the Upper Permian Emeishan continental flood basalts, Southwestern China. Int. Geol. Rev. 43, 213–225.
Song, X.-Y., Zhou, M.-F., Cao, Z.-M., Robinson, P.T., 2004. Late Permian rifting of the South China Craton caused by the Emeishan mantle plume? J. Geol. Soc. 161, 773–781.
Song, X.-Y., Qi, H.-W., Robinson, P.T., Zhou, M.-F., Cao, Z.-M., Chen, L.-M., 2008a. Melting of the subcontinental lithospheric mantle by the Emeishan mantle plume; evidence from the basal alkaline basalts in Dongchuan, Yunnan, Southwestern China. Lithos 100, 93–111.
Song, X.-Y., Zhou, M.-F., Tao, Y., Xiao, J.-F., 2008b. Controls on the metal compositions of magmatic sulfide deposits in the Emeishan large igneous province, SW China. Chem. Geol. 253, 38–49.
Song, X.-Y., Keays, R.R., Xiao, L., Qi, H.-W., Ihlenfeld, C., 2009. Platinum-group element geochemistry of the continental flood basalts in the central Emeishan large igneous province, SW China. Chem. Geol. 262, 246–261.
Song, X.-Y., Qi, H.-W., Hu, R.-Z., Chen, L.-M., Yu, S.-Y., Zhang, J.-F., 2013. Formation of thick stratiform Fe–Ti oxide layers in layered intrusion and frequent replenishment of fractionated mafic magma: evidence from the Panzhihua intrusion, SW China. Geochem. Geophys. Geosyst. 14, 712–732.
Tanaka, T., Togashi, S., Kamioka, H., Amakawa, H., Kagami, H., Hamamoto, T., Yuhara, M., Orihashi, Y., Yoneda, S., Shimizu, H., 2000. JNdi-1: a neodymium isotopic reference in consistency with LaJolla neodymium. Chem. Geol. 168, 279–281.
Tao, Y., Li, C., Hu, R., Ripley, E.M., Du, A., Zhong, H., 2007. Petrogenesis of the Pt–Pd mineralized Jinbaoshan ultramafic intrusion in the Permian Emeishan large igneous province, SW China. Contrib. Mineral. Petrol. 153, 321–337.
Tao, Y., Li, C., Song, X.-Y., Ripley, E.M., 2008. Mineralogical, petrological, and geochemical studies of the Limahe mafic–ultramatic intrusion and associated Ni–Cu sulfide ores SW China. Mineral. Deposita 43, 849–872.
Taylor, H.P., 1967. Oxygen isotope studies of hydrothermal mineral deposits. In: Barnes, H.L. (Ed.), Geochemistry of Hydrothermal Ore Deposits, pp. 109–142 (New York).
Turner, F., 1965. Note on the genesis of brucite in contact metamorphism of dolomite. Contrib. Mineral. Petrol. 11, 393–397.
Valley, J.W., 1986. Stable isotope geochemistry of metamorphic rocks. In: Valley, J.W., Taylor, H.P., O'Neil, J.R. (Eds.), Stable Isotopes in High Temperature Processes. Rev. Mineral. Geochem 16, pp. 445–489.
Wang, C.Y., Zhou, M.-F., 2013. New textural and mineralogical constraints on the origin of the Hongge Fe–Ti–V oxide deposit SW China. Mineral. Deposita 48, 787–798.
Wang, C.Y., Zhou, M.-F., Qi, L., 2007. Permian flood basalts and mafic intrusions in the Jinping (SW China)–Song Da (northern Vietnam) district: mantle sources, crustal contamination and sulfide segregation. Chem. Geol. 243, 317–343.
Wang, C.Y., Zhou, M.-F., Zhao, D., 2008. Fe–Ti–Cr oxides from the Permian Xinjie mafic–ultramafic layered intrusion in the Emeishan large igneous province, SW China: crystallization from Fe- and Ti-rich basaltic magmas. Lithos 102, 198–217.
Wilson, S.A., 1998. Data compilation and statistical analysis of intralaboratory results for AGV-2. U.S. Geological Survey Open-File Report.
Xiao, L., Xu, Y.G., Mei, H.J., Zheng, Y.F., He, B., Pirajno, F., 2004. Distinct mantle sources of low-Ti and high-Ti basalts from the western Emeishan large igneous province SW China: implications for plume–lithosphere interaction. Earth Planet. Sci. Lett. 228, 525–546.
Xu, Y.-G., Chung, S.-L., Jahn, B.-M., Wu, G., 2001. Petrologic and geochemical constraints on the petrogenesis of Permian–Triassic Emeishan flood basalts in southwestern China. Lithos 58, 145–168.
Xu, Y.-G., He, B., Chung, S.-L., Menzies, M.A., Frey, F.A., 2004. Geologic, geochemical, and geophysical consequences of plume involvement in the Emeishan flood-basalt province. Geology 32, 917–920.
Xu, Y.-G., Luo, Z.-Y., Huang, X.-L., He, B., Xiao, L., Xie, L.-W., Shi, Y.-R., 2008. Zircon U–Pb and Hf isotope constraints on crustal melting associated with the Emeishan mantle plume. Geochim. Cosmochim. Acta 72, 3084–3104.
Zhang, Z., Mahoney, J.J., Mao, J., Wang, F., 2006. Geochemistry of picritic and associated basalt flows of the western Emeishan flood basalt province China. J. Petrol. 47, 1997–2019.
Zhang, X.-Q., Song, X.-Y., Chen, L.-M., Xie, W., Yu, S.-Y., Zheng, W.-Q., Deng, Y.-F., Zhang, J.-F., Gui, S.-G., 2012. Fractional crystallization and the formation of thick Fe–Ti–V oxide layers in the Baima layered intrusion SW China. Ore Geol. Rev. 49, 96–108.
Zhao, Z.-F., Zheng, Y.-F., 2003. Calculation of oxygen isotope fractionation in magmatic rocks. Chem. Geol. 193, 59–80.
Zheng, Y.-F., 1990. Carbon–oxygen isotopic covariation in hydrothermal calcite during degassing of CO_2. Mineral. Deposita 25, 246–250.
Zheng, Y.-F., 1991. Calculation of oxygen isotope fractionation in metal oxides. Geochim. Cosmochim. Acta 55, 2299–2307.
Zheng, Y.-F., 1993. Calculation of oxygen isotope fractionation in anhydrous silicate minerals. Geochim. Cosmochim. Acta 57, 1079–1091.
Zhong, H., Zhou, X.-H., Zhou, M.-F., Sun, M., Liu, B.-G., 2002. Platinum-group element geochemistry of the Hongge Fe–V–Ti deposit in the Pan-Xi area, southwestern China. Mineral. Deposita 37, 226–239.
Zhong, H., Yao, Y., Prevec, S.A., Wilson, A.H., Viljoen, M.J., Viljoen, R.P., Liu, B.-G., Luo, Y.-N., 2004. Trace-element and Sr–Nd isotopic geochemistry of the PGE-bearing Xinjie layered intrusion in SW China. Chem. Geol. 203, 237–252.
Zhong, H., Qi, L., Hu, R.-Z., Zhou, M.-F., Gou, T.-Z., Zhu, W.-G., Liu, B.-G., Chu, Z.-Y., 2011. Rhenium–osmium isotope and platinum-group elements in the Xinjie layered intrusion, SW China: implications for source mantle composition, mantle evolution PGE fractionation and mineralization. Geochim. Cosmochim. Acta 75, 1621–1641.
Zhou, M.-F., Yan, D.-P., Kennedy, A.K., Li, Y., Ding, J., 2002a. SHRIMP U–Pb zircon geochronological and geochemical evidence for Neoproterozoic arc-magmatism along the western margin of the Yangtze Block South China. Earth Planet. Sci. Lett. 196, 51–67.
Zhou, M.-F., Malpas, J., Song, X.-Y., Robinson, P.T., Sun, M., Kennedy, A.K., Lesher, C.M., Keays, R.R., 2002b. A temporal link between the Emeishan large igneous province (SW China) and the end-Guadalupian mass extinction. Earth Planet. Sci. Lett. 196, 113–122.
Zhou, M.-F., Robinson, P.T., Lesher, C.M., Keays, R.R., Zhang, C.-J., Malpas, J., 2005. Geochemistry, petrogenesis and metallogenesis of the Panzhihua gabbroic layered intrusion and associated Fe–Ti–V oxide deposits, Sichuan Province, SW China. J. Petrol. 46, 2253–2280.
Zhou, M.-F., Arndt, N.T., Malpas, J., Wang, C.Y., Kennedy, A.K., 2008. Two magma series and associated ore deposit types in the Permian Emeishan large igneous province, SW China. Lithos 103, 352–368.
Zhou, M.-F., Chen, W.-T., Wang, C.-Y., Prevec, S.A., Liu, P.-P., Howarth, G.H., 2013. Two stages of immiscible liquid separation in the formation of Panzhihua-type Fe–Ti–V oxide deposits, SW China. Geosci. Front. 4, 481–502.